

ANALYSIS AND MODELING OF EDGE EFFECTS THAT ARISE IN THE  
RAMAN SPECTRUM OF A SILICON WAFER

BY  
A. FIORILLO

A Thesis

Submitted to the Division of Natural Sciences  
New College of Florida  
in partial fulfillment of the requirements for the degree  
Bachelor of Arts  
Under the sponsorship of Professor Mariana Sendova, Ph.D.

Sarasota, Florida  
May, 2015

## Acknowledgements

The work contained herein is the largest and most comprehensive single project I've worked on to date. This project has occupied the forefront of my mind for nearly three years and condensing it into this thesis has been challenging academically, emotionally, and physically. I would not have been able to finish, much less start, it without the invaluable guidance and inexhaustible patience of wonderful teachers and compassionate friends.

In particular, Drs. Mariana Sendova and Brian Hosterman both inspired me to begin this project and provided countless hours of patient assistance. Dr. Don Colladay provided some of the most stirring insights I've ever encountered in physics, and he did so with jokes that are elegantly hilarious. Dr. Steven Shipman showed me that it is in fact possible to be a good scientist *and* a good human. These professors simply did their job – they taught me a lot of physics (and a little bit of chemistry) – but they did it generously, effortlessly, and *well*.

# Contents

Acknowledgements	ii
Contents	iii
List of Figures	iv
Abstract	v
Introduction	1
<b>1 Physical Context</b>	<b>3</b>
1.1 The Interaction of Light and Matter . . . . .	3
1.2 The Raman Effect . . . . .	5
1.3 Raman Microscopy . . . . .	8
1.4 Simplified Coordinate System . . . . .	11
<b>2 Experimental Methods</b>	<b>13</b>
2.1 Cleaving & Wafer Preparation . . . . .	13
2.2 Collecting Raman Spectra and Performing Line Scans . . . . .	14
2.3 Automated Peak Fitting . . . . .	16
<b>3 Data &amp; Analysis</b>	<b>18</b>
3.1 Edge Scans . . . . .	18
3.2 Slits . . . . .	24
3.3 Edge Scans with Varied Cleavage Planes . . . . .	26
<b>4 Numerical Models</b>	<b>30</b>
4.1 Convolved Fresnel Diffraction . . . . .	31
4.2 Beam Falling off Edge . . . . .	33
4.3 Edge Enhanced Simulation . . . . .	36
<b>5 Conclusion</b>	<b>41</b>
<b>Appendix Fityk Script Generator</b>	<b>43</b>
<b>Appendix “Peaks”</b>	<b>46</b>
<b>Appendix Edge Enhanced Model</b>	<b>49</b>

# List of Figures

1.1	The unit cell of mono-crystalline silicon . . . . .	6
1.2	Raman spectrum of mono-Si . . . . .	7
1.3	Two cleavage planes of a mono-Si crystal . . . . .	8
1.4	Resolution limits of a compound microscope . . . . .	10
1.5	Objective lens properties . . . . .	10
1.6	One-dimensional approximation of experimental setup . . . . .	11
2.1	Picture of experimental setup . . . . .	15
2.2	Picture of cleaved edge . . . . .	15
3.1	50X line scans over various edges . . . . .	20
3.2	10X and 100X line scans over various edges . . . . .	22
3.3	100X line scans over slits of variable width . . . . .	25
3.4	Atomic density of different cleavage planes for mono-Si . . . . .	27
3.5	Line scans over (110) edges . . . . .	29
4.1	Simulation of Fresnel diffraction model . . . . .	33
4.2	Beam-falling-off-an-edge model simulation . . . . .	35
4.3	Simulations of the Edge Enhanced model using varied parameters. The chosen values for $\omega$ correspond to the available objectives using Eq. (4.4) and Table 1.5. The other parameter ranges were chosen after fitted to data. . . . .	38
4.4	Fiting with the Edge Enhanced model . . . . .	39

ANALYSIS AND MODELING OF EDGE EFFECTS THAT ARISE IN THE  
RAMAN SPECTRUM OF A SILICON WAFER

A. Fiorillo

New College of Florida, 2014

ABSTRACT

The intensity of mono-crystalline silicon's  $522\text{ cm}^{-1}$  Raman mode is observed as a function of position  $I_{522}(x)$  across the physical edge of a wafer. In the region near the edge, the intensity is enhanced up to 80% greater than the intensity observed on the wafer's interior. This enhancement is characterized empirically through the analysis of over 14 line scans. Three models are constructed to simulate the results of  $I_{522}(x)$ . The most effective model is analogous to an error function over three distinct regions along the line scan: interior silicon, the physical edge, and no-silicon. The simulations correlate well with experimental results and suggest potential applications in the detection of edges.

Mariana Sendova

Division of Natural Sciences

# Introduction

Mono-crystalline silicon (mono-Si) has a relatively narrow primary Raman band centered at  $522\text{ cm}^{-1}$  with a width of about  $6.64\text{ cm}^{-1}$ . A material's Raman spectrum, at fixed excitation laser intensity, provides characteristic information about the crystalline and molecular properties. The simple spectrum of silicon is partly a result of its diamond cubic crystal structure.

An emergent phenomenon is observed when many Raman spectra are collected along a line crossing the edge of a silicon wafer. The intensity of the  $522\text{ cm}^{-1}$  mode  $I_{522}$  is plotted as a function of  $x$ , i.e.  $I_{522}(x)$ . In this plot, an enhancement of up to 80% (with respect to the average intensity at the wafer's interior) is observed near the physical edge. The position of greatest intensity varies with the spectrometer's spot size and the wavelength of the excitation laser.

This curious effect has been observed by a team of researchers at Iowa State University.<sup>1</sup> The researchers concluded that the intensity enhancement is due to *nano*-crystalline grains near the edge (with respect to the interior). The slight widening of the band and leftward shift of the band's center are also attributed to the change nano-crystalline grain size. Ultimately, the enhancement of  $I_{522}(x)$  is suggested as a method to characterize grain size.

The purpose of this project is to establish the empirical relationships that describe the behavior of this enhancement  $I_{522}(x)$ . Three distinct models are constructed and evaluated with regard to their empirical consistency. The most successful model uses numerical simulation to predict the enhancement using very basic principles of Raman scattering.

*Many* (over 10,000) spectra were collected for this project. Automated processing

---

<sup>1</sup>Xu et al. (2013) is one of a small handful of articles which mention the effect at all.

techniques were developed to assist in handling such a great volume of data.

Before discussing the finer details of the project, the first chapter is written to provide the physical context of the experiment. The basis of the Raman effect is discussed, leading into an explanation of Raman spectroscopy. The optical properties of microscopic systems and laser beams are also examined. Not intended to be a full treatment of either subject, the chapter introduces terminology and a coordinate system used to visualize the experiment.

The next chapter details the experimental setup and procedure used to collect Raman spectra. The methods for preparing samples and processing spectra are also clearly defined. Finally, the Python programs used to automate spectrum processing are outlined, as are the details of peak fitting.

The results of 14 line scans over edges, as well as 4 line scans over “slits,” are presented in the Data & Analysis chapter. Scans were performed by varying three primary experimental parameters: microscope objective, excitation wavelength, and cleavage plane of the edge. The enhancement appears to vary depending on each of these parameters.

In the Models chapter, three attempts to explain the enhancement of  $I_{522}(x)$  are discussed. The first of these attributes the effect to diffraction. The other two models suggest that the enhancement is a result of the interaction between a Gaussian excitation beam and the different surfaces probed. The third model specifically suggests that the edge’s face is the primary source of enhancement.

At this point, however, it is appropriate to start with the basics.

# Chapter 1

## Physical Context

This chapter contains a brief summary of the physics necessary to explain the context of the experiment and potential sources of the enhancement. To begin, it is appropriate to discuss the Raman effect and its (many) applications in solid state physics and the materials science. Following a basic introduction to Raman scattering, consideration is given to the light sources being used and compound microscope systems. The remainder of this chapter will include an explicit simplification of the experiment's geometry.

### 1.1 The Interaction of Light and Matter

Some of the most commonly discussed results of quantum mechanics offer useful descriptions of how light interacts with matter. Two particularly useful points are:

- Light is quantized into massless particles called photons. The energy  $E_\gamma$  of photons is proportional to frequency  $\nu$  or wavelength  $\lambda$  of the light, i.e.  $E_\gamma = h\nu = \frac{hc}{\lambda}$  where  $h$  is Planck's constant and  $c$  is the speed of light in a vacuum. It is common (especially in spectroscopy) to relate a photon's energy to its wavenumber  $\tilde{\nu} = \frac{1}{\lambda}$ , namely  $E_\gamma = hc\tilde{\nu}$ .
- Rather than orbiting an atom in a planetary fashion, electrons occupy orbitals of differing shapes, distances from the nucleus, and potential energies. A serious quantum mechanical treatment of atomic orbitals is well beyond the scope of

this discussion.<sup>1</sup> Suffice it to say that electrons may only exist with discrete energies, and the transition between these energy levels is nearly instantaneous (on the order of microseconds).

When a photon “strikes” an atom, the photon is absorbed and its energy is “donated” to the atom. The atom is “excited,” and the atom’s electrons are promoted to higher-energy orbitals. This absorption process applies specifically when the energy of the incident photon is nearly equal to the energy difference between two energy levels in the recipient atom. When the incident photon’s energy does not correspond neatly to the excitation energies (differences between allowed energy levels), electromagnetic scattering occurs.

Light is scattered from an atomic collision essentially because the incident photon’s energy could not be comfortably absorbed by the atom’s orbital structure.<sup>2</sup> Scattering phenomena can be broken into two main types based on the overall change in energy: elastic scattering occurs when the incident photon has the same energy as the scattered photon, and inelastic scattering is when the scattered photon has a different energy. The law of conservation of energy implies that inelastically scattered light somehow “donates” (or “steals”) energy from the collision.

This model of interaction between light and atoms is easily extended to the interaction between light and molecules. With molecules, however, in addition to exciting electrons (electronic modes) to higher orbitals, the inter-atomic bonds themselves can become excited. The inter-atomic bonds are often modeled as quantized harmonic oscillators – the potential between atoms is approximated as a spring. The natural frequencies that result from this model correspond to available vibrational modes. Thus when light interacts with a molecule, the vibrational and electronic modes both contribute to the interaction. If the incident photon’s energy neatly fits within one of the available modes, it is absorbed by the molecule, otherwise it is scattered.

---

<sup>1</sup>Though an excellent introduction to quantum mechanics is Griffiths (2005).

<sup>2</sup>The specifics of this quick re-emission process involve a perturbation of the orbital structure, causing an oscillating dipole, and the radiation of a photon. For more details, see Long (2002).

The preferential absorption of certain energy bands in the infrared is used to characterize molecular properties – i.e. IR spectroscopy.<sup>3</sup> An alternative method of analyzing the vibrational modes of molecules is to analyze the inelastically scattered light. The discovery and characterization of this type of scattering earned Sir Chandrasekhara Venkata Raman the 1930 Nobel Prize in Physics.<sup>4</sup>

## 1.2 The Raman Effect

In a crystal lattice, atoms are bonded together in a repeating pattern.<sup>5</sup> The smallest representation of a lattice’s pattern is called the unit cell. The unit cell of mono-crystalline silicon, is shown in Fig. 1.1. Every atom in the lattice is a silicon atom, each is separated by the lattice constant  $a = 0.542 \text{ nm}$ .<sup>6</sup>

The bond between each of the atoms in the crystal can be modeled as harmonic oscillators (just as in the last section’s treatment of inter-atomic bonds). In the limit of many atoms, the crystal lattice is treated as an enormous three-dimensional system of coupled oscillators. Each of these atoms oscillates about a mean position with some frequency  $\nu_i$ . If every atom in the lattice is vibrating at the same frequency (a normal mode), the lattice itself exists in a collectively excited state. In the quantized model, these excited states are represented by *phonons* and indeed have discrete energies!<sup>7</sup>

Depending on whether the oscillators within the lattice are in-phase or out-of-phase with each other, these collective excitations are classified as acoustic or optical modes, respectively. When light interacting with a crystal “donates” (or “steals”) energy corresponding to one of the optical modes, *Raman* scattering occurs.<sup>8</sup> Optical phonons have typical energies on the order of meV.

---

<sup>3</sup>Reusch (2013)

<sup>4</sup>C.V. Raman’s Nobel Lecture is available on the nobelprize.org website and is an historically interesting read, Raman (1930).

<sup>5</sup>Certain molecules may also be arranged into a crystalline solid, such as CO<sub>2</sub>, however we are primarily interested in atomic crystals here.

<sup>6</sup>NIST (2010)

<sup>7</sup>See Kittel (2004), Mathew (2006), or Long (2002) for *much* more detail on the development of phonon theory.

<sup>8</sup>Misra (2011)

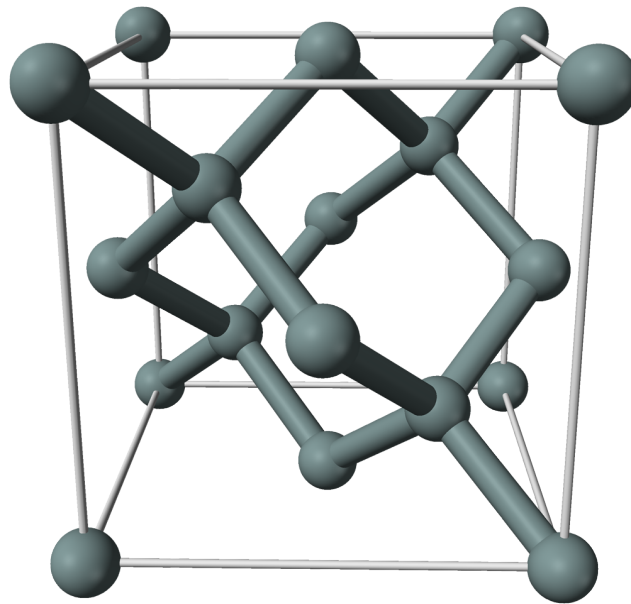


Figure 1.1: Mono-crystalline silicon forms a diamond cubic structure. The lattice constant of  $a = 0.5430710$  nm has been measured to impressive precision by NIST. Image credit goes to Ben Mills.

The Raman effect can be observed in practice by directing a monochromatic  $E_\gamma = E_0$  (at wavenumber  $\nu_0$ ) source of photons at some material and measuring the spectrum of the back-scattered light. The spectrum of back-scattered light includes a very large peak at  $\nu = \nu_0$  (Rayleigh scattered) and smaller peaks at  $\nu = \nu_0 \pm \Delta\nu$  (Raman scattered). The Raman spectrum is the intensity of back-scattered light  $I$  as a function of Raman shift  $\Delta\nu$ .<sup>9</sup>

The peaks of the Raman spectrum are indicative of the allowed optical modes of the lattice. A characteristic Raman spectrum of silicon is presented in Fig. 1.2. Mono-crystalline silicon possesses one primary band at  $\Delta\nu = 522.5 \pm 0.01$  cm $^{-1}$ , corresponding to a phonon energy of  $\approx 64.7$  meV. The spectral width of this band, the full width at half maximum, FWHM =  $6.649 \pm 0.014$  cm $^{-1}$  is somewhat narrow.

---

<sup>9</sup>This expression can further be broken into two more finely defined types of Raman scattering. *Stokes* Raman scattering corresponds to scattered photons with energy less than the incident beam (i.e.  $\nu = \nu_0 - \Delta\nu$ ). *Anti-Stokes* Raman scattering corresponds to the opposite ( $\nu = \nu_0 + \Delta\nu$ ). Stokes and Anti-Stokes Raman scattered light are mostly symmetric about  $\nu_0$ , though in most experimental conditions Stokes transitions tend to be more intense – see Long (2002). The spectra shown throughout this project are a superposition of Stokes and Anti-Stokes transitions.

In more complex materials, multiple bands of varying widths may exist; silicon is remarkable for its comparatively *simple* Raman spectrum. The Raman bands relate back to the vibrational modes of the lattice and can be used to infer many interesting material characteristics.<sup>10</sup>

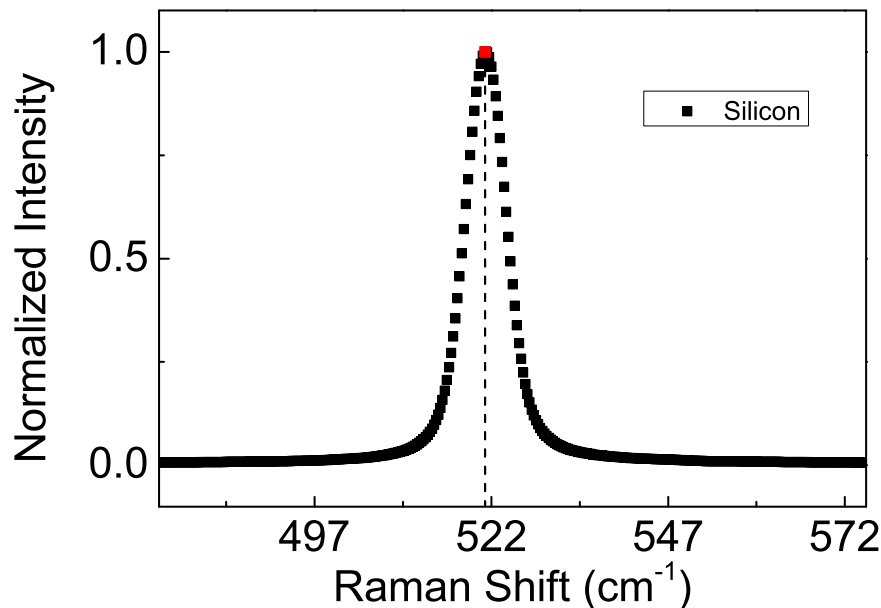


Figure 1.2: The primary Raman band of silicon at  $\Delta\nu \approx 522 \text{ cm}^{-1}$ . The intensity of this band is referred to as  $I_{522}$ .

The principal focus of this project, however, is *not* to characterize silicon by looking at a single Raman spectrum. Rather, an emergent phenomenon observed by analyzing *many* Raman spectra is the principal focus of this project. Up to this point, the goal of this chapter has been to provide sufficient context to interpret the Raman spectrum of silicon. Hereon, the primary feature of importance is the maximum intensity of silicon's primary band. It will be referred to often, so it should be quite clear that  $I_{522}$  refers to this peak intensity.

At this point it is possible to justify the two main reasons that silicon is the only material being analyzed in this project.

1. Silicon has one Raman band and it is straightforward to determine the parameters

---

<sup>10</sup>Kittel (2004) goes into further detail on normal modes and Raman selection criteria.

of this band using a computer. The suite of Python scripts written for this project were mostly created for this purpose. A collection of the most crucial subroutines are included in the Appendix. The details of spectral analysis, and its automation, are discussed in the next chapter.

2. A silicon crystal may be cleaved along one of these three planes to produce a very straight edge. Two of these cleavage planes are displayed in Fig. 1.3. By analyzing a sample with a nearly ideal edge, the enhancement of  $I_{522}$  across that edge may be more carefully characterized.

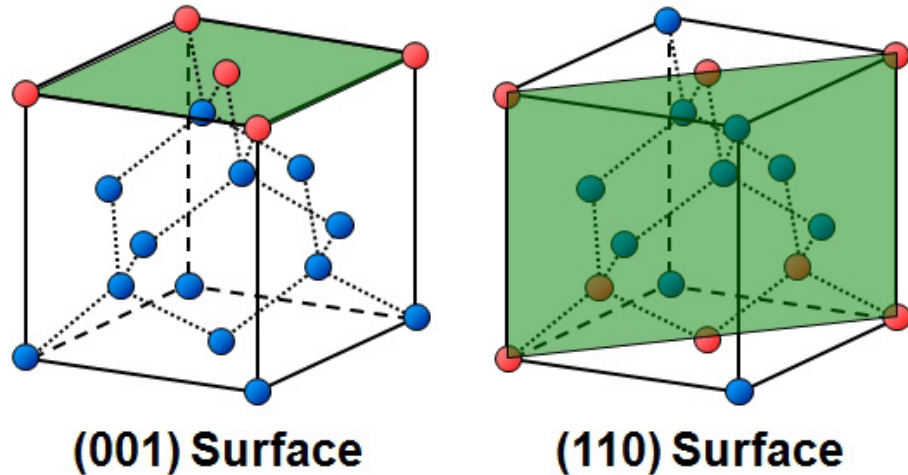


Figure 1.3: Two of the three main lattice planes in a silicon crystal. Each represents the family of parallel planes within the lattice, labeled by the Miller index. Image credit goes to Fujitsu (2008).

### 1.3 Raman Microscopy

The apparatus used to capture the silicon Raman spectra is specifically a Raman *microscope* made by Kaiser Optical Systems, Inc. The device uses a compound optical microscope to guide the excitation laser's incident light and also to capture the backscattered light.<sup>11</sup> This section characterizes several important properties of

---

<sup>11</sup>The backscattered light is analyzed using a spectrometer fitted with a holographic diffraction grating and a cooled CCD detector.

this microscopic system, chief of which is the “spot.” The “spot” is the region on which the microscope is focused and the *only* region from which Raman signals are measured.<sup>12</sup>

The spot size of the micro-probe  $d$  indicates the diameter of this roughly circular region, called the field of view. Determining the spot size, either by calculation or by direct measurement, is not trivial.

In a compound microscope system, the objective lens determines the system’s magnification. The smallest resolvable distance  $d_{xy}$  between any two points (on the sample) is related to the excitation laser’s wavelength  $\lambda$  and the numerical aperture NA of the objective, i.e.

$$d_{xy} = \frac{\lambda}{2\text{NA}} . \quad (1.1)$$

The  $xy$  subscript indicates that these two points are on the  $xy$ -plane, implicitly defining the  $z$ -axis along the axis of the objective.<sup>13</sup> With a limit on resolvable distance, a simple measurement of the spot size immediately becomes difficult.

This resolution limit is fundamentally due to diffraction. The diffraction pattern that results from a single microscopic point is called an Airy disk; its functional representation is called the point-spread function. When two microscopic points are very close together, the principal maxima of their respective Airy disks merge. The minimum distance between the two principal maxima  $d_{xy}$  is called the Rayleigh criterion. Two very illustrative diagrams published in Zeiss’ Microscopy Library are combined in Fig. 1.4.

Despite the difficulty in measuring an exact spot size, it is possible to estimate it through conventional means. The Kaiser Optical Systems operation manual provides a table with the estimated spot sizes that correspond to several objectives. The relevant entries from this table are quoted in Table 1.5.

The excitation laser itself has some nontrivial profile (intensity distribution in space) which further complicates the estimation of a spot size. Many models of the

---

<sup>12</sup>Kaiser Optical Systems operation manual

<sup>13</sup>Rottenfusser, Wilson, and Davidson (Rottenfusser et al.)

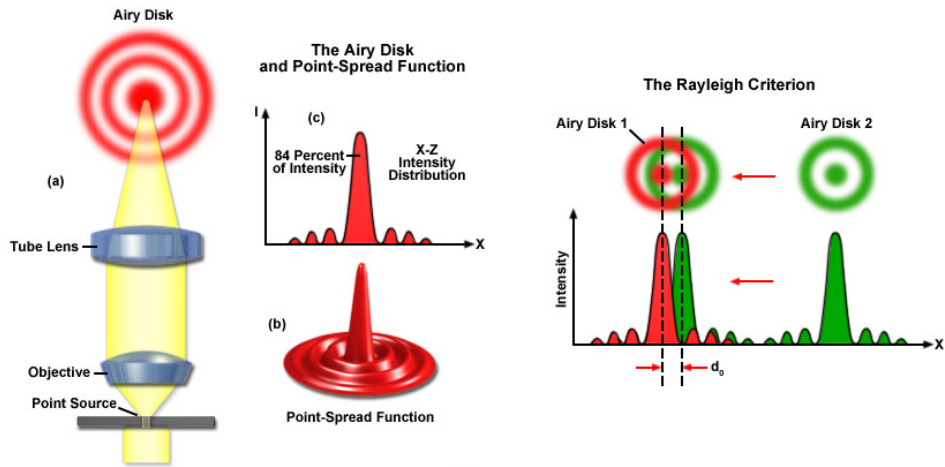


Figure 1.4: Left: (a) shows the airy disk being detected by a magnified point source, (b) is a 3D representation of the point-spread function, (c) shows the point-spread function along the  $xz$ -plane where  $y = 0$ . Right: two Airy disks merge when the distance between their respective point sources is smaller than  $d_{xy}$ . Image credit goes to Rottenfusser et al. (n.d.).

Description	NA	Working distance (mm)	Spot size ( $\mu\text{m}$ )
10X	0.25	5.8	50
50X	0.75	0.37	10
100X	0.9	0.27	5

Figure 1.5: Tabulated properties of the objectives used in this experiment. Working distance indicates the distance between the surface of the front lens on the objective. The spot sizes are specifically labeled as “approximate” by the Kaiser Optical Systems operation manual.

beam profile have been studied elsewhere<sup>14</sup>, however the two in consideration for this project are: (a) approximately Gaussian, and (b) circular “top-hat.”

If, indeed the profile is approximately Gaussian, then what is the minimum excitation intensity to detect a Raman signal? For an unmagnified laser beam, the full width at tenth maximum, FWTM is a conventional measure of spot size.<sup>15</sup> For the purpose of this project, this convention is extended to the microscopic system.

<sup>14</sup>Siegman (1997)

<sup>15</sup>Wright et al. (1992)

## 1.4 Simplified Coordinate System

This section is concerned with the mathematical treatment of the experiment's geometry. The natural experimental configuration's geometry is in three dimensions and depends largely on the intersection between a radial Gaussian-like beam and an edge. It became very clear in the early stages of this project that analysis should take place in a simplified coordinate system (shown in Fig. 1.6).

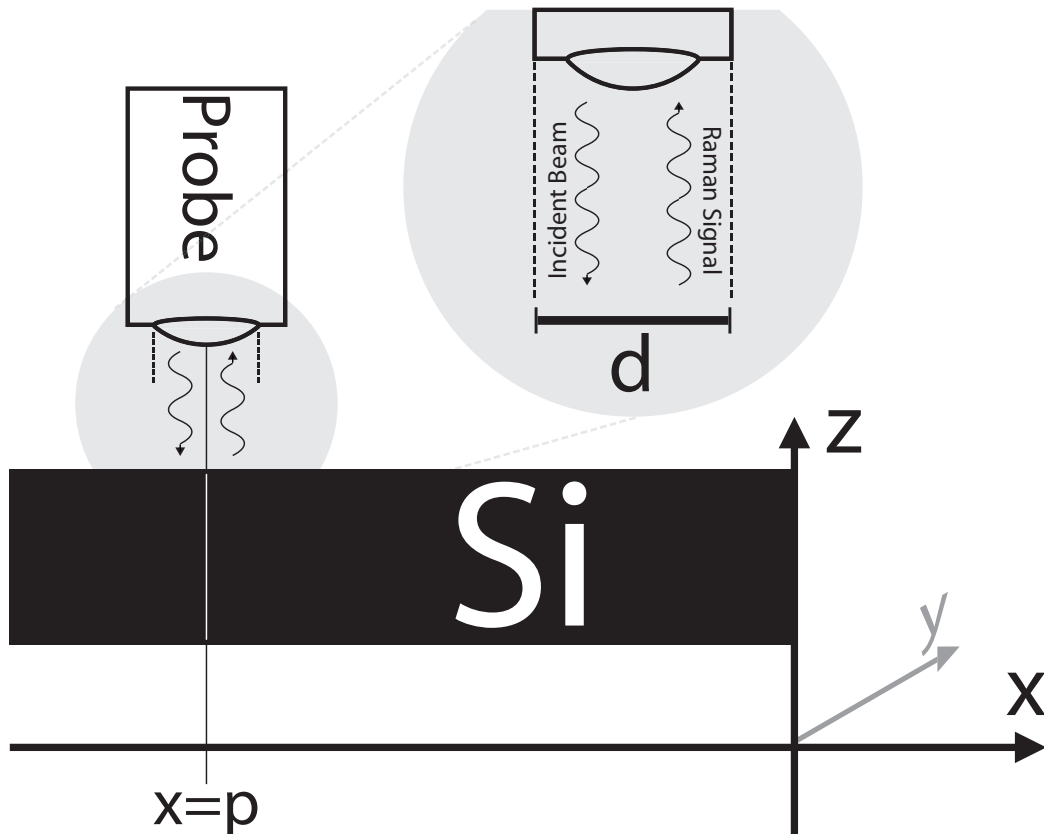


Figure 1.6: The beam profile is reduced from a radial function to a slice along the  $xz$ -plane ( $y = 0$ ).  $d$  indicates the spot size, often the FWTM, of the beam and  $p$  indicates the spot's center. The physical edge extends along the  $y$ -axis (into/out of the page).

The biggest simplification made is the reduction to two dimensions. This is justified by the radial symmetry present in both beam profile models. The intensity of the beam is either constant over the spot's area (circular “top hat”) or decreases radially from the spot's center. Given a such function  $z = f(x, y) = f(r)$ , the 2D

slice of highest excitation energy is along the  $xz$ -plane ( $y = 0$ ). The intensity of the back-scattered Raman signal is proportional to the incident beam's intensity, so this slice also indicates the dominant source of Raman back-scattering.<sup>16</sup>

Notable flaws in this simplification include entirely ignoring potentially significant slices near the  $xz$ -plane ( $y \neq 0$ ). The relative significance of these slices is not fully clear, though they are higher order contributions.

It is also possible that this 2D model ignores Raman scattered light with an angular component – i.e. the path of the scattered light is *not* co-axial with the  $z$ -axis. The objective acceptance angle depends on magnification<sup>17</sup> however under experimental conditions this angle is quite small. Using values quoted from Table 1.5, this is at most  $\theta \approx 0.01^\circ$ .

This simplified coordinate system does, however, provide a simple way to identify important features of the beam. Additionally, it makes visual the interaction of the probe's spot with the silicon edge. The line scans discussed throughout this project are collected from spectra taken as a function of  $x$ , i.e. the center of the beam  $p$  is shifted along this line.

The intensity of silicon's primary Raman mode was earlier expressed as  $I_{522}$ . The function  $I_{522}(x)$  thus compactly expresses this intensity as a function of position. An enhancement is observed in the plot of  $I_{522}(x)$  in the region near the edge. This enhancement has been observed by others<sup>18</sup> and under various experimental configurations.

This project's main goal is to identify, characterize, and suggest an explanation for the enhancement of  $I_{522}(x)$ . In this chapter, Raman scattering and optical microscopy were discussed to give the physical context in which this enhancement has been observed. A simplified coordinate system has also been established. It is now appropriate to move on to the specific experimental procedure used to characterize this effect.

---

<sup>16</sup>Long (2002)

<sup>17</sup> $\tan(\theta) = (d/2L)$  where  $L$  is the working distance and  $d$  is the spot size.

<sup>18</sup>Xu et al. (2013)

# Chapter 2

## Experimental Methods

The purpose of this chapter is to detail the procedure for cleaving a silicon wafer, for collecting Raman spectra, and for configuring a line scan. Additionally, the software used to automate peak fitting is described and a flowchart illustrates the analysis work flow. The majority of these methods were established and refined with Dr. Brian Hosterman.

### 2.1 Cleaving & Wafer Preparation

The mono-crystalline silicon wafers used for this project were acquired through University Wafer. Most wafers analyzed have a nominal thickness of  $280\ \mu\text{m}$  and a lattice plane orientation of [001]. One set of line scans involved a “thick” wafer with a nominal thickness of  $500\ \mu\text{m}$  and an orientation of [001]. Two additional wafers, both of nominal thickness  $\approx 300\ \mu\text{m}$ , with orientations [110] and [111] were purchased through El-Cat. All wafers are undoped and are single side polished.

Before cleaving, a mask is placed over the wafer to match the wafer’s cleavage plane. A diamond scribe is used to etch the wafer along the mask. A pair of tweezers is then used to hold the larger half of the wafer in place. The wafer is snapped along the scribed edge. An illustrative tutorial of this process is given by Prime Wafers, and a useful reference for silicon’s crystalline properties is given by Nova Electronic Materials.<sup>1</sup>

Once cleaved, the wafer sections are dusted and cleaned with a lab tissue and

---

<sup>1</sup>Prime Wafers (2015) and Nova Electronic Materials (2014)

isopropanol. Cleaved wafers are stored in small plastic cases with a cushion of lab tissue. In preparation of capturing spectra, wafers are *delicately* handled with a pair of tweezers or gloved hands and are cleaned again with isopropanol.

## 2.2 Collecting Raman Spectra and Performing Line Scans

The primary apparatus used throughout this project is a Raman microscope, produced by Kaiser Optical Systems. The microscope possesses three objective lenses – a 10X, 50X, and 100X – which briefly are characterized by the product manual. The specific properties of these lenses are tabulated in Table 1.5. Part of the apparatus also includes an experimental stage that can be adjusted in three dimensions in increments of approximately  $0.1 \mu\text{m}$ . This adjustment is controlled by the lab computer and is essential to performing line scans.

The GRAMS software suite, created by Thermo Scientific, is used to collect Raman spectra and to control the stage. For every spectrum, the software outputs a spectrum file in a proprietary format and the  $(X, Y, Z)$  coordinates of the stage with respect to a manually calibrated origin. In preparation of analysis, each spectrum file is converted into a plain text file<sup>2</sup> using the GRAMS Converter Tool.

The parameters of a line scan are configured and automated using GRAMS. The cleaved wafer's primary flat is positioned normal to the incident beam and held in place by a sample holder firmly attached to the experimental stage. A photograph of the experimental configuration is shown in Fig. 2.1.

The microscope's camera is used to find a relatively featureless region near the wafer's edge and the coordinate origin for the scan is set to the edge – an example of this calibration is shown in Fig. 2.2. Using the video interface, an origin is established (edge at  $x = 0$ ) and the x-axis is chosen perpendicular to the edge ( $x < 0$  region is interior,  $x > 0$  region has *no silicon*).

---

<sup>2</sup>They are space-delimited with two columns: Raman shift ( $\text{cm}^{-1}$ ) and Intensity (arbitrary units).

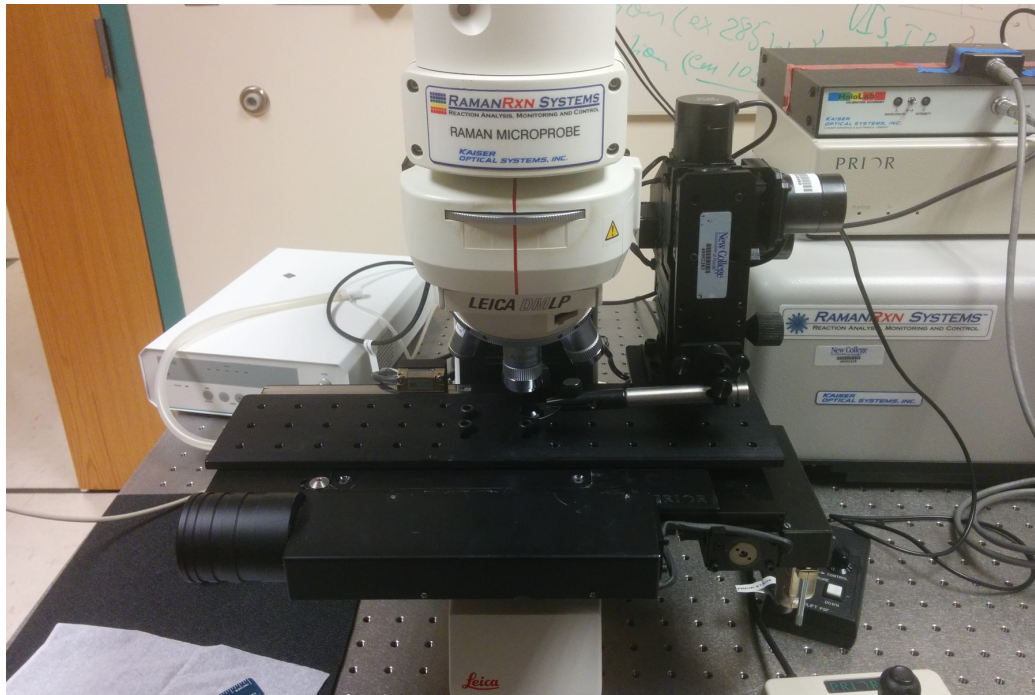


Figure 2.1: Picture of the Raman Microprobe set up for a line scan across an edge. The nanomanipulator is connected to the experimental stage by a black metal adapter. The sample holder is holding a silicon wafer under the objective.

The line scan is configured by specifying a starting point, and ending point, and the number of spectra to acquire. Most line scans traverse the straight line between  $(-100 \mu\text{m}, 0, 0)$  and  $(+100 \mu\text{m}, 0, 0)$  in increments of  $0.5 \mu\text{m}$ .

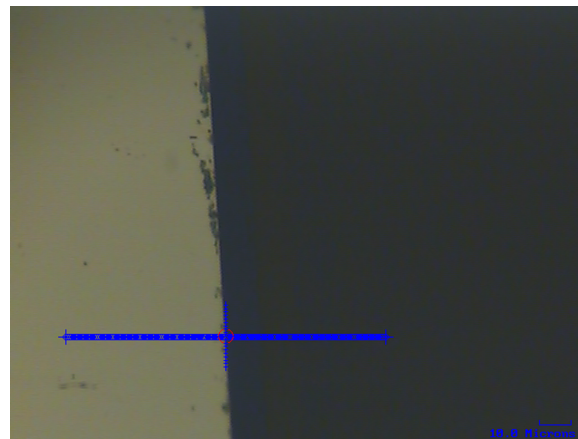


Figure 2.2: A microscope camera's picture of a candidate edge for a line scan. The cross hairs indicate the origin.

In addition to performing line scans across silicon edges, several line scans across

“slits” are performed. A “slit” is simply two silicon edges (prepared as before) positioned very close to each other, as close as  $1\text{ }\mu\text{m}$ .

The “first” edge is oriented exactly as is done with a single-edge line scan. Using an electronic nanomanipulator firmly attached to the experimental stage, the “second” edge is positioned adjacent to the affixed edge. The slit width is measured using the video interface in GRAMS. Using this method, slit scans were performed with widths ranging from  $1\text{ }\mu\text{m}$  to  $50\text{ }\mu\text{m}$ .

## 2.3 Automated Peak Fitting

Each line scan yields approximately 400 spectrum files and a text file containing each file’s respective coordinates. Initially, the goal was to scan most edges four times (two scans in each direction, “on-to-off” and “off-to-on”), ideally with each of the three objective lenses, and examine at least eight different physical edges. This set the expected number of spectra to analyze at approximately 38,000, each of which to be fitted to a Voigt beam profile and whose fitted parameters are used to calculate the area under the peak and uncertainties. Clearly an automated process for processing these spectra is needed!

The program used for peak fitting is Fityk<sup>3</sup>, written by Marcin Wojdyl, and was chosen for this purpose due to its robust scripting language. It has a built-in function for the Voigt profile, given by Eq. (2.1), and offers many output options of the optimized parameters (including height  $a_0$ , center  $a_1$ , shape  $a_3$ , and gwidth  $a_4$ ).

$$y = a_0 \frac{\int_{-\infty}^{+\infty} \left[ \frac{e^{-x^2}}{a_3^2 + \left( \frac{x-a_1}{a_2} - x \right)^2} \right] dx}{\int_{-\infty}^{+\infty} \left[ \frac{e^{-x^2}}{a_3^2 + x^2} \right] dx} \quad (2.1)$$

Fortunately, Fityk’s scripting language allows the entire fitting process (for *simple* curves) to be automated for an arbitrary number of spectra, ultimately outputting one text file containing each spectrum’s fitted parameters.

---

<sup>3</sup>Wojdyl (2010) and Wojdyl (2014)

The *FitykScriptGenerator* Python program given in the appendix generates Fityk scripts by iterating over this procedure for each spectrum:

1. Open spectrum file
2. Set active range and (if using the Fityk's GUI) adjust the visible plot accordingly
3. Define a baseline function by collecting several points outside of the peak's region
4. Subtract the baseline from all data points
5. Insert a Voigt profile near the peak
6. Run Fityk's fitting algorithm many times
7. Export peak's fitted parameters as a line in the specified output file
8. Close spectrum file

After fitting each spectrum, the Fityk output file is processed with the *\_peaks*<sup>4</sup> Python program. This final step reconstructs the array to be easily opened with Microsoft Excel or OriginLab and, more importantly, calculates the area under the Voigt curve, as well as parameter uncertainties.

---

<sup>4</sup>This script has functions written in to calculate uncertainties for each peak parameter.

# Chapter 3

## Data & Analysis

This chapter will summarize the results of over 15 line scans across the distinct edges of silicon. Common features observed in plots of  $I_{522}(x)$  will be identified and characterized. Scans were performed using three different objectives (10X, 50X, and 100X) and two excitation wavelengths (532 nm and 785 nm). Additionally, line scans across slits of varying width will be analyzed in a similar fashion. Edges 1-10<sup>1</sup> are all from [001] wafers, whereas subsequent edges have varying lattice orientation. In order to evaluate the numerical models described in the next chapter, we must develop more precise terms to describe the enhancement of  $I_{522}(x)$ .

Over 10,000 spectra were collected and processed in connection with this project. These line scans are derived from that *large* collection of Raman spectra. Each data point shown in Fig. 3.1a, for instance, originates from a particular Raman spectrum of silicon.

### 3.1 Edge Scans

There are several notable features common to line scans over a single edge using objectives with a small spot size (i.e. 50X and 100X,  $d \approx 10 \mu\text{m}$  and  $\approx 5 \mu\text{m}$  respectively). These features are labeled in Fig. 3.1a and identified using red points. Their labels are:

**A** is the first point where  $I_{522} \approx 1.1$ ,

---

<sup>1</sup>This numbering is for clerical purposes and is used as a shorthand to refer to each “edge scan.”

**B** is the point of maximum  $I_{522}$ ,

**C** is the second point where  $I_{522} \approx 1.1$  again,

**D** corresponds to the point nearest the physical edge  $x \approx 0$ ,

**E** is the point where  $I_{522} \approx 0.5$ .

In Figs. 3.1 and 3.2 the same features (if present) are also identified using red points.

The “meta-peak” is the enhancement of  $I_{522}$  with which this project is concerned. The term “meta-peak” also sometimes refers to the *point* of maximum  $I_{522}$ , i.e. point **B**. The position difference between **A** and **C** gives a value used to characterize the width of the enhancement, that is the full width at tenth maximum (“meta-FWTM”). The “meta-FWTM” is represented in Fig. 3.1a as a cyan line between points **A** and **C**.

The features of each plot shown in Fig. 3.1 are tabulated in Table 3.1.

Edge #	A (Left 110%)		B (“Meta-Peak”)		C (Right 110%)		D (Edge)		E (50%)	
	x ( $\mu\text{m}$ )	$I_{522}$								
1	-14.1	1.102	-3.5	1.802	-0.5	1.119	0.0	0.9524	1.2	0.5357
2	-13.0	1.108	-2.5	1.794	0.3	1.160	0.0	1.324	2.3	0.5204
3	-10.6	1.010	-1.4	1.631	2.0	1.101	0.0	1.573	4.3	0.4550
4	-	-	-9.9	1.062	-	-	0.1	0.01336	-5.3	0.5101
5	-	-	-11.8	1.061	-	-	0.0	0.0081	-7.5	0.4809

Table 3.1: Tabulated coordinates of the features identified in Fig. 3.1. These results are from scans with the 50X objective and with [001] oriented wafers. Edges 1-3 were scanned with an excitation wavelength of 785 nm; Edges 4 & 5 are with excitation wavelength 532 nm.

The first, and possibly most significant, observation is the large “meta-peak” observed in scans with the 785 nm beam (Figs. 3.1a to 3.1c). Comparatively small “meta-peaks” are observed in scans with the 532 nm excitation wavelength (Figs. 3.1d and 3.1e).

The average “meta-peak” for the 785 nm beam scans is 1.74 (with range<sup>2</sup> 0.171), whereas the average for the scans with the 532 nm beam is 1.06 (range 0.001).

<sup>2</sup>By “range,” I am reporting the difference between the maximum and minimum observed values. This is reported in lieu of a standard deviation due to the small number of scans

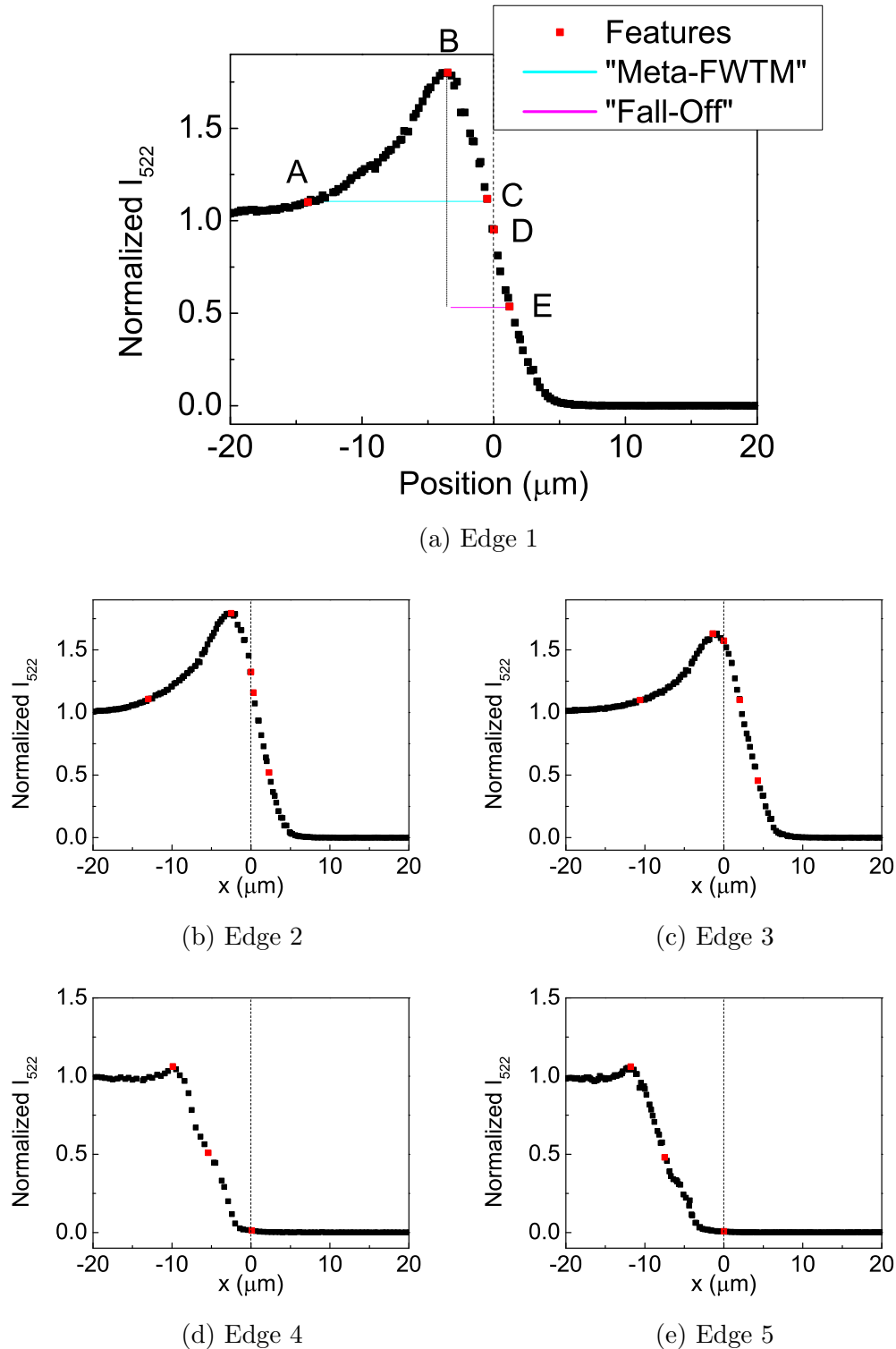


Figure 3.1: The results of several line scans using the 50X objective lens and with two excitation wavelengths (“beams”), 785 nm shown in (a) to (c) and 532 nm shown in (d) and (e).

Since Edges 4 & 5 don't exhibit a strong enhancement, they do not have well-defined "meta-FWTMs." Edges 1-3, however, have an average "meta-FWTM" of  $13.2 \mu\text{m}$  (range  $1.0 \mu\text{m}$ ).

Another descriptive feature is the position difference between the "meta-peak" and the point of  $I_{522} \approx 0.5$ , i.e. between **B** and **E**. This difference is represented by a magenta line on Fig. 3.1a and is termed the "fall-off." The "fall-off" provides a measure of how steep<sup>3</sup> the drop in  $I_{522}(x)$  is. A shorter "fall-off" indicates a steeper drop in  $I_{522}(x)$  and vice versa. The average "fall-off" for Edges 1 - 3 is  $5.1 \mu\text{m}$  (range  $1.0 \mu\text{m}$ ). Likewise, for Edges 4 & 5 the average "fall-off" is  $4.5 \mu\text{m}$  (range  $0.3 \mu\text{m}$ ).

Line scans using the other two available objectives were also performed using the 785 nm beam, the results of which are shown in Fig. 3.2. Similar features as described above are observed in scans with the 100X objective, however the "fall-off" is smaller (avg.  $1.5 \mu\text{m}$ , range  $0.0 \mu\text{m}$ ) and the "meta-peak" is smaller (avg.  $1.50$ , range  $0.0640 \mu\text{m}$ ) than seen in the scans with the 50X objective. The 100X scans have an average "meta-FWTM" of  $6.2 \mu\text{m}$  (range  $0.4 \mu\text{m}$ ) which is comparable to the 50X scans.

Scans performed with the 10X objective lens do not have clearly distinguishable "meta-peaks." Additionally, 10X scans have a larger "fall-off" (avg.  $6.6 \mu\text{m}$ , range  $1.6 \mu\text{m}$ ) compared to scans performed with the 50X or 100X objectives. The features of the 10X and 100X scans shown in Fig. 3.2 are tabulated in Table 3.2.

Edge #	A (Left 110%)		B ("Meta-Peak")		C (Right 110%)		D (Edge)		E (50%)	
	x ( $\mu\text{m}$ )	$I_{522}$								
6	-	-	-24.3	1.027	-	-	0.0	0.7558	5.8	0.5352
7	-	-	-22.8	1.024	-	-	-0.2	0.7706	7.4	0.4801
8	-6.1	1.108	-2.1	1.469	-0.1	1.052	-0.1	1.052	1.4	0.5014
9	-8.0	1.086	-3.0	1.533	-1.6	1.143	-0.1	0.4502	-0.1	0.4502

Table 3.2: Tabulated coordinates of the features identified in Fig 3.2. These scans were all performed with an incident beam wavelength of 785 nm. The dashed boxes for Edges 6 & 7 indicate a lack of those features.

<sup>3</sup>Steepness is usually more precisely defined as slope  $\frac{\Delta y}{\Delta x}$ . Here, however  $\Delta y$  is always negative, so "fall-off" gives an approximate and *inverse* measure of the slope.

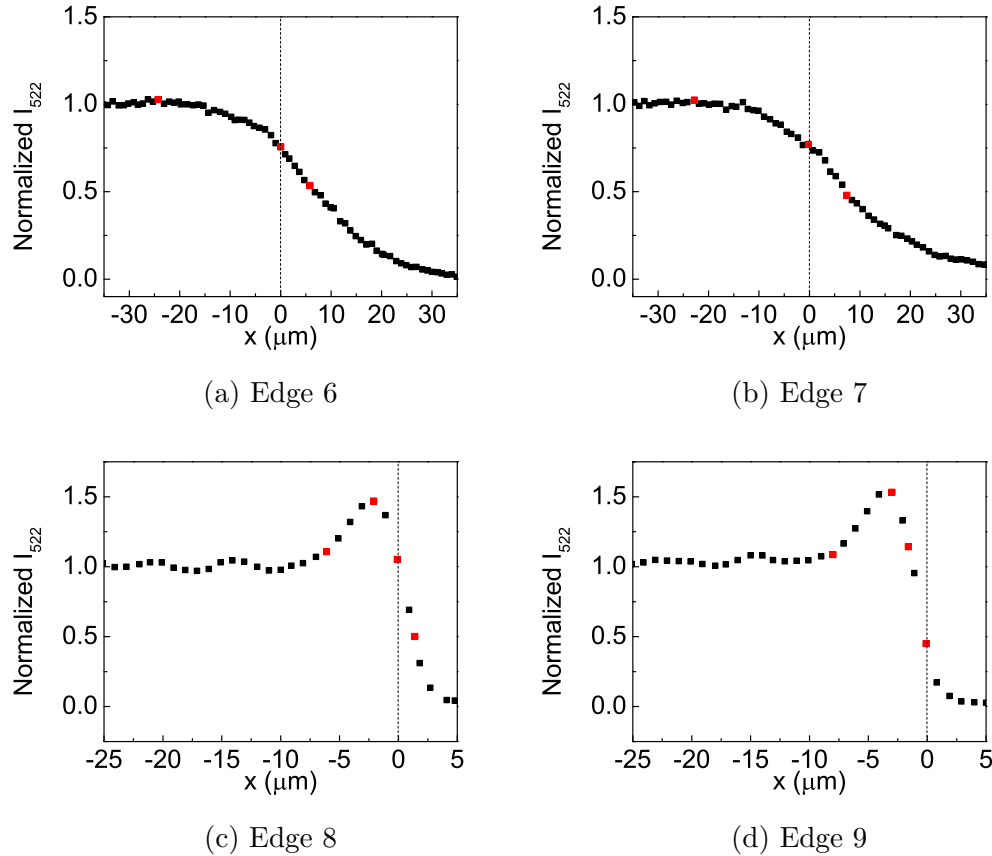


Figure 3.2: Characteristic line scans with the 10X and 100X objective lenses. With the 10X objective, no notable enhancement is observed. With the 100X objective, a stronger enhancement than is seen in 50X scans is observed.

In several of the scan-pairs<sup>4</sup> shown above, it seems at first glance that the features are not strongly correlated. The “meta-peak,” for example, observed in Edges 1-3 is observed at quite different distances from the respective cleaved edge ( $x = 0$ ). Since the “fall-offs” agree quite well, however, this seems to imply that some scans are slightly offset from the calibrated origin (i.e. the cleaved edge) during collection.

The emergent features for each of the above scans – “meta-peak,” “meta-FWTM,” and “fall-off” – are tabulated in Table 3.3.

Each of the averages given above are calculated from only a small number of scans (at most three). As such, any inferences made regarding the enhancement of  $I_{522}(x)$  ought to be made cautiously.

<sup>4</sup>Pairs of scans performed with the same excitation wavelength and objective.

Edge #	Objective	Beam (nm)	“Meta-Peak”	“Meta-FWTM” ( $\mu\text{m}$ )	“Fall-Off” ( $\mu\text{m}$ )
1	50X	785	1.802	13.6	4.7
2			1.794	13.3	4.8
3			1.631	12.6	5.7
4	50X	532	1.062	-	4.6
5			1.061	-	4.3
6	10X	785	1.027	-	5.8
7			1.024	-	7.4
8	100X	785	1.469	6.0	1.5
9			1.533	6.4	1.5

Table 3.3: Summary of emergent features observed in the enhancement of  $I_{522}(x)$ .

With due caution, a few empirical statements about the behavior of  $I_{522}(x)$  seem to be:

1. There is a positive relationship between the “meta-peak” and the excitation wavelength, i.e. longer wavelength corresponds with a larger “meta-peak.” This can be seen quite clearly in a comparison between Edges 1 - 3 with Edges 4 & 5.
2. There is negative relationship between the “meta-peak” and the spot size. The scans performed with the 10X objective lens ( $d = 50 \mu\text{m}$ ) show no “meta-peak,” whereas the 100X scans ( $d = 5 \mu\text{m}$ ) clearly have an enhancement of  $I_{522}(x)$ .
3. There is a positive relationship between the “fall-off” and the spot size. 100X scans “fall-off” in about  $1.5 \mu\text{m}$ , whereas 10X scans “fall-off” in as much as  $7.4 \mu\text{m}$ .

These statements are called “empirical” because they are formed specifically to summarize the results of the above line scans. The relationships listed above are consistent with the line scans performed on Edges 1-9 and they provide testable predictions.

In the next chapter, several distinct models are used to develop numerical simulations to mimic the enhancement observed in  $I_{522}(x)$ . The “goodness” of each model is evaluated qualitatively using a sort of heuristic argument. If the model’s simulation is consistent with these empirical relationships, it is effective. In order to construct a

model of the  $I_{522}(x)$  enhancement with practical applications, however, these empirical relationships must be refined.

The analysis of line scans with experimental parameters distinct from those seen in Edges 1-9 occupy the remainder of this chapter. Certain experimental parameters so far unconsidered, i.e. the cleaved wafer's orientation, reveal additional empirical relationships.

At this point, however, sufficient context has been provided to justify the development of each model in the next chapter. Each associated simulation's initial construction was guided by the relationships observed in line scans similar to those in Edges 1-9. In the context of these edges, the primary experimental variables are the objective and the wavelength of the excitation laser.

## 3.2 Slits

Line scans principally similar to those discussed in the previous section were performed using a “slit” configuration (i.e. two silicon edges positioned some slit width  $w$  from each other). At first glance, the results appear to be a superposition of two edges, with features very similar to those characterized above. It has been observed, however, with very small slits ( $w < 5 \mu\text{m}$ ) the “meta-peaks” of both edges merge. This single “meta-peak” often occurs when the beam's center is not on silicon at all, but in fact over empty space! An example of this beginning to happen is seen in Fig. 3.3d.

The line scans performed on slits were all done with a 100X objective lens and with identical edge pairs, only the slit width is varied. The results of these scans are shown in Fig. 3.3.

In some line scans over slits, different “meta-peaks” were observed for each edge. It is possible that this indicates a connection between the “meta-peak” and surface characteristics of the silicon's edge. However, it is also possible that the “second” edge's position (with respect to the “first” edge) is behind this effect.

Most slit scans performed in connection with this project extend the results of the previous section's scans (Edges 1-9) in a straightforward fashion. Edges 8 & 9

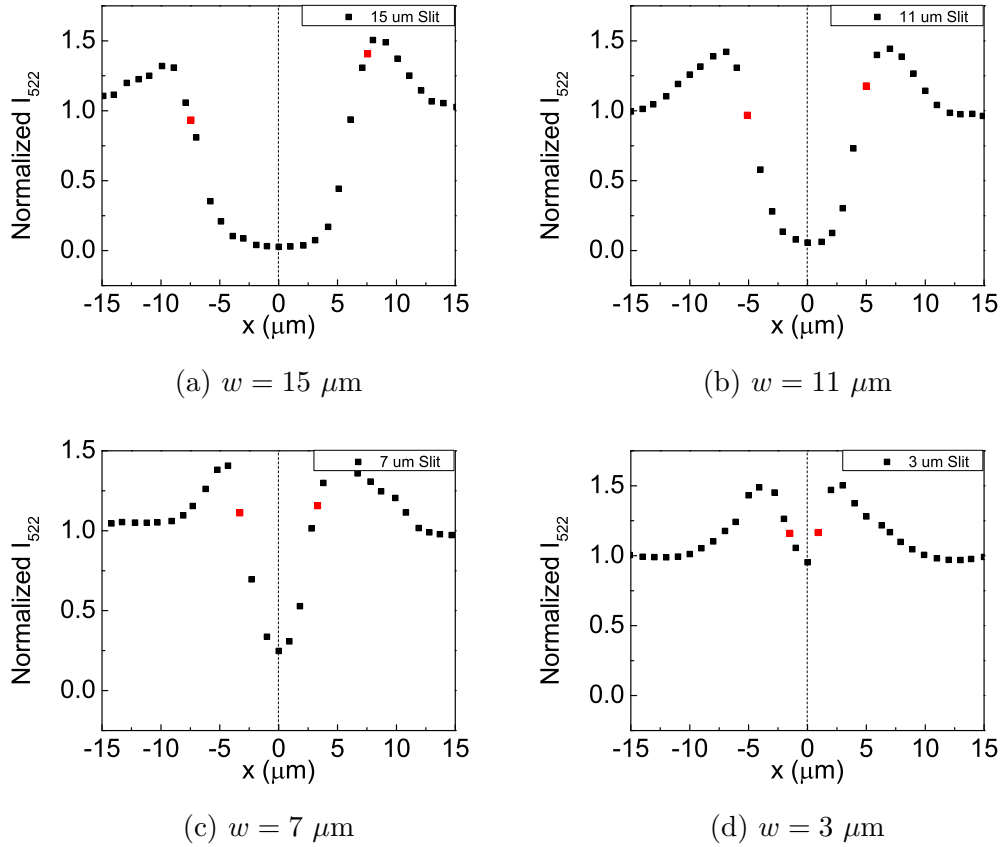


Figure 3.3: Scans performed with the 100X objective lens and 785 nm excitation wavelength. The red points here indicate each cleaved edge.

(see Figs. 3.2c and 3.2d), in fact, are plotted using points collected from the “first” edge in the  $15 \mu\text{m}$  and  $13 \mu\text{m}$  slits shown above, respectively. For slit widths larger than the spot size ( $w > 5 \mu\text{m}$  for the 100X objective), the enhancement of  $I_{522}(x)$  behaves in much the same way as a single edge. An “meta-peak” is observed near both edges using the 50X<sup>5</sup> and 100X objectives. The respective “fall-offs” are also consistent with the result of edge scans.

The most interesting result from slit scans occurs only with very narrow slits ( $w < d$ ). In this regime, when the center of the probe’s spot coincides with the center of the slit, segments of the spot are focused on three regions: (a) the “first” edge, (b) the empty space between the edges, and (c) the “second” edge. Only regions (a) and

<sup>5</sup>Slit scans were performed using each of the available objectives. Only the 100X slit scans are reported here due to the limited numerical simulations performed for a slit configuration.

(c) contribute a Raman signal, and the Raman signal observed from these regions is in fact *more intense* than the normalized Raman signal of either wafer. This trend is observable in the scans presented in Fig. 3.3.

This result is common to all (sufficiently narrow) slit scans performed with the 50X and 100X objectives. The enhancement of  $I_{522}(x)$  due to narrow slits is, if unexpected, a very provocative result. In the preliminary stages of this project, many more slit scans were performed than are presented here.<sup>6</sup> The conclusion of this extended focus on slit scans is this: apparently, there is some interaction between the probe and the edges which enhances the observed Raman signal's intensity *substantially*.

The enhancement is clearly due to the interaction between the probe and a silicon edge, at least in part. When two edges are probed simultaneously (as in a narrow slit configuration), the enhancement is much more intense, but the experimental setup is also doubly complicated. In the hope of determining the underlying cause of this “edge enhancement,” research efforts were rededicated to edge scans. Models designed to simulate the enhancement due to single edge can be additionally tested with slit configurations.

### 3.3 Edge Scans with Varied Cleavage Planes

In discussion of this project, Dr. Sendova suggested that the cleavage plane (the plane which makes up the edge’s “face”) could play a role in the enhancement of  $I_{522}(x)$ . This suggestion evolved out of the observation that the different cleavage planes have a different surface density of silicon atoms and of Si-Si lattice bonds. This is illustrated in a diagram published on the El-Cat.com website, shown in Fig. 3.4. The number of silicon atoms and the number of Si-Si bonds, both *per unit cell* (i.e. surface densities), are counted up from Figs. 3.4 and 1.1 and tabulated in Table 3.4.

---

<sup>6</sup>Well over 30 distinct slit scans, and their spectra were processed accordingly. The number of spectra collected per slit scan nearly double than similar edge scans, often around 400 spectra per slit scan. The total number of spectra collected and processed for these slit scans is conservatively estimated at 10,000.

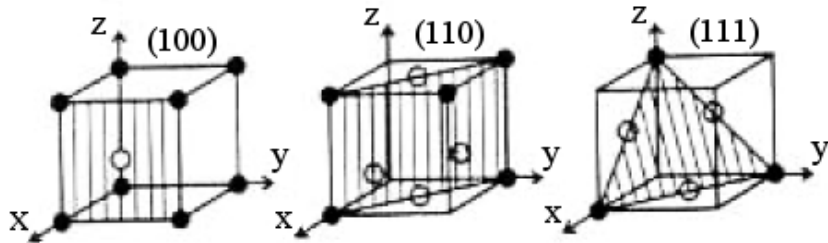


Figure 3.4: The primitive unit cell of mono-crystalline silicon cleaved along three planes, identified by their Miller indices<sup>7</sup>. The silicon atoms within the cleaved plane are represented by shaded (corner atoms) and un-shaded (face and interior atoms) spheres. Image credit to Sikora (2011).

Plane	Si Atoms Cell	$\left( \frac{10^{14} \text{ Si Atoms}}{\text{cm}^2} \right)$
(100)	2	6.78
(110)	4	9.59
(110)	2	7.83

Table 3.4: Each of the cleavage planes shown in Fig. 3.4 possess a different density of silicon atoms. Details of this counting method are given in Kittel (2004).

A new hypothesis was developed in discussing Dr. Sendova’s observation: do the varying plane densities (either atomic- or Si-Si bond-) along the cleaved edge “face” contribute to the enhancement of  $I_{522}(x)$ ? And, if so, to what extent? It stands to reason that if more silicon is “seen” by the probe’s spot (i.e., the spot is focused on a region with comparatively higher silicon density), a more intense Raman signal will be detected.

This delightfully elegant explanation of the enhancement’s nature has, at the time of writing, been modeled with some success. Presently, additional line scans are being performed across edges that were cleaved to have (110) and (111) planes.

Before presenting the results of these new line scans, it is essential to clarify the two planes of interest in this project. The “slice plane” of a wafer is the surface of largest area on an un-cleaved wafer. In the experimental geometry shown in Fig. 1.6 this plane indicates the surface whose normal vector is ideally co-axial with probe’s spot (i.e. Miller index of (001)). The edge is created by cleaving along the respective wafer’s cleavage plane.<sup>8</sup> The cleaved edge’s face *is* this plane, with the corresponding

<sup>8</sup>Dicing patterns for various wafer orientations are given by Sikora (2011).

Miller index and surface densities.

Note: for the [100] oriented wafers, the cleaved edge has a Miller index of (100) and the “slice plane” has a Miller index of (001). In many texts, these planes are treated synonymously (because of their obvious symmetry). In the context of this experiment, though, they are *distinct*.

Two wafers with lattice orientations [110] and [111] were acquired to answer questions regarding the impact of lattice orientation on the “meta-peak” and other enhancement properties. The thickness of these new “alternative orientation” wafers is  $\approx 300 \mu\text{m}$  – comparable to the thickness of the wafers from Edges 1-9 ( $\approx 285 \mu\text{m}$ ). Additionally, these alternative orientation wafers share the same single-side polish (SSP) and are undoped mono-crystalline silicon.

Both wafers were cleaved and scanned according to the same procedure as Edges 1-5<sup>9</sup>, i.e. with a 50X objective and the 532 nm & 785 nm excitation wavelengths. Edges 1 - 5, however, are different in that their edge planes have Miller indices (100).

Edges 11-14 refer to line scans performed on different edges<sup>10</sup> of the [110] oriented wafer. At the time of writing, no scans have been performed on the [111] oriented wafer, however at least two edge scans (21 & 22) are planned.

The line scans for Edges 11-14 are shown in Fig. 3.5. The features of  $I_{522}(x)$ , in the same format as Edges 1-9, are tabulated in Table 3.5. Edges 11 & 12 were collected with an excitation wavelength of 532 nm; Edges 13 & 14 with the 785 nm beam.

Edge #	A (Left 110%)		B (“Meta-Peak”)		C (Right 110%)		D (Edge)		E (50%)	
	x ( $\mu\text{m}$ )	$I_{522}$								
11	-	-	-8.6	1.014	-	-	-0.1	0.05391	-5.0	0.5125
12	-	-	-18.0	1.000	-	-	0.0	0.5229	0.0	0.5229
13	-19.4	1.103	-7.1	1.256	-4.6	1.095	0.0	0.1076	-2.1	0.4852
14	-7.5	1.1050	-2.8	1.195	-1.1	1.098	-0.1	0.9697	1.6	0.5381

Table 3.5: Tabulated coordinates of the features identified in Fig 3.5.

<sup>9</sup>See Figs. 3.1a through 3.1e.

<sup>10</sup>Actually, the scans were performed using a single cleaved edge to conserve cost and reduce the risk of error in sample preparation. The “different edges” refer to different sites along the same cleaved edge.

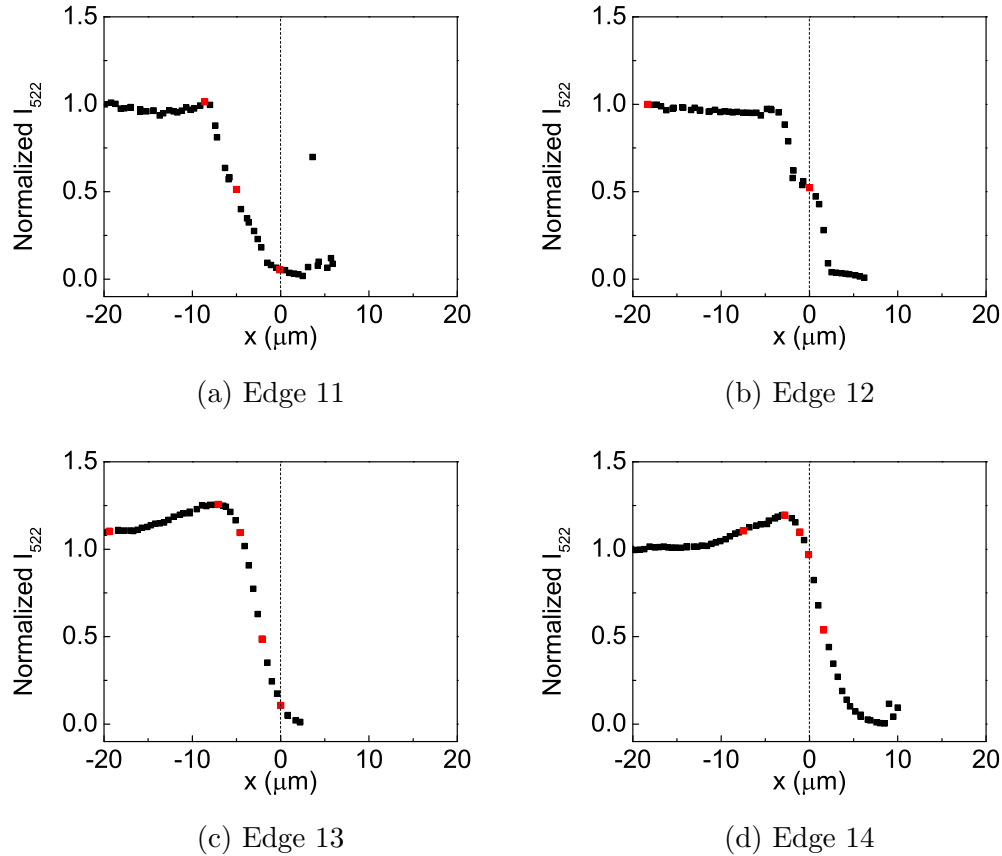


Figure 3.5: Line scans performed with a 50X objective. The primary contrast between Edges 4 & 5 and those shown here is the wafer orientation, i.e. [001] and [110] respectively.

It is clear in the line scans of Edges 11 & 12 that there's no distinguishable “meta-peak” and with Edges 13 & 14, the peaks are much smaller than observed with the (100) edges. Much larger “meta-FWTMs” are also observed in Edges 13 & 14 than their counterparts (Edges 1-3).

In the next chapter, the data presented here will be compared to numerical simulations. An effective model will be able to account for the experimental parameters we varied in this chapter: objective (i.e. spot size), excitation wavelength, and orientation (i.e. surface atomic density).

# Chapter 4

## Numerical Models

This chapter summarizes the three most developed models of  $I_{522}(x)$ . The final model constructed for this project is by far the most effective. Details regarding its formulation, refinement, and empirical consistency occupy the latter portion of this chapter. Before jumping to the success, however, it is appropriate to make explicit the scale of this project. In the context of the project-as-a-whole, the evolutionary steps between models are thus revealed.

The tacit ambition that motivated the adoption and advancement of this project is to explain the underlying mechanism of a somewhat obscure physical phenomenon (i.e. the enhancement of  $I_{522}(x)$ ). To this end, over the course of nearly three years: tens of thousands of Raman spectra were collected, automation schemes were devised to process & collect individual spectra into line scans, emergent properties from these line scans were catalogued, and several empirical relationships governing the enhancement of  $I_{522}(x)$  have been deduced through careful variation of experiment parameters.

Over the roughly the same three year period countless explanations of  $I_{522}(x)$  have been postulated, many of them either overlapping or at odds with each other. After some concerted guesswork, two promising (and contradictory) branches of reasoning emerged:

- The enhancement of  $I_{522}(x)$  is observed near edges and slits because its cause is rooted in diffraction.
- The enhancement is observed is *not* diffraction-based. Instead, the observed

Raman signal is related to the interface between the microprobe's spot and the surface of the silicon wafer.

The first model constructed with any testable implications was based on the diffraction hypothesis. Subsequent, and more effective, models were constructed based on the contrary hypothesis – i.e. the interface between the probe spot and silicon surface is the primary interaction behind the enhancement of  $I_{522}(x)$ .

## 4.1 Convolved Fresnel Diffraction

When the space between a light source and the viewing plane is obstructed by an opaque half-screen, a fringe pattern is observed. If the half-screen is close to the viewing plane, these fringes are a result of Fresnel diffraction.<sup>1</sup>

This model is principally on an analogy between the experimental setup and the conventional configuration Fresnel diffraction occurs due to an edge. The silicon wafer translates to a roughly monochromatic light source of plane waves. The  $I_{522}$  parameter measured from each spectrum actually corresponds to roughly monochromatic light<sup>2</sup> and the experimental configuration allows only backscattered light (i.e. plane waves along the [001] orientation). In a region where the probe is “off of the edge” with no sample to excite, there is no  $I_{522}$  signal to detect. In this region, the absence of an  $I_{522}$  signal is an analogous result to that observed by placing the detector behind an opaque screen.

The approximations made in constructing this analogy are sound enough for cursory analysis. The analog-orientation was framed to resemble the already solved problem of Fresnel diffraction due an edge. Conveniently, the position of the cleaved edge is the same in the experimental- and analog-orientations, i.e.  $x = 0$ .

Michael Richmond performed numerical simulations of Fresnel diffraction, but in the context of lunar occultations.<sup>3</sup> As the Moon orbits the Earth, the lunar disk

<sup>1</sup>Hecht (2002)

<sup>2</sup>The Stokes and Anti-Stokes Raman bands are minor deviations from monochromatic approximation.

<sup>3</sup>Richmond (2005)

observed on the planet's surface traverses the “celestial sphere.” As the lunar disk’s edge approaches a distant star, the star’s light is diffracted and fringes can be detected on the Earth’s surface. In principal, Richmond solved an interesting astronomical problem using the solutions for Fresnel diffraction due to an edge.

The basic problem analyzed by Richmond uses the same fundamental configuration and interaction (i.e. Fresnel Edge-diffraction) as our analog-orientation. Thus, at least for cursory analysis, the simulations reported by Richmond are compared to the results analyzed in the previous chapter.

Richmond applied the condition of Fresnel diffraction to an intensity integral over the screen, then evaluated the integral numerically for many values of  $x$ . The intensity of the fringes  $I(x)$  are expressed:

$$\begin{aligned} I(x) &= I_0 \left| \int_{-\infty}^x e^{\left(\frac{i\pi u^2}{L\lambda}\right)} du \right|^2 \\ &= I_0 \left( \left| \int_{-\infty}^x \cos \left( \frac{\pi u^2}{L\lambda} \right) du \right|^2 + \left| \int_{-\infty}^x \sin \left( \frac{\pi u^2}{L\lambda} \right) du \right|^2 \right) \end{aligned} \quad (4.1)$$

where  $I_0$  is normalized to some interior intensity,  $L$  is the distance between the viewing screen and the obstruction,  $\lambda$  is the wavelength of the light being diffracted, and  $I(x)$  gives the intensity fluctuations resulting from diffraction fringes.

One particularly interesting conclusion of Richmond’s is this: “If we can measure accurately the intensity of the first fringe ... and the intensity of the star far from the shadow’s edge [normalized interior intensity  $I_0$ ], we can use the ratio of intensities to guess at the angular size [of the star].” In the context of a silicon edge’s Raman spectrum, this conclusion would suggest a similar model can be used to detect the physical edge to high accuracy.

The results of a characteristic simulation are shown in Fig. 4.1, and many more are given on Richmond’s website. While initially promising, it’s clear that the higher-order fringes apparent in this model are not obvious in the results described in the previous chapter. Specifically, Richmond provides a condition which predicts

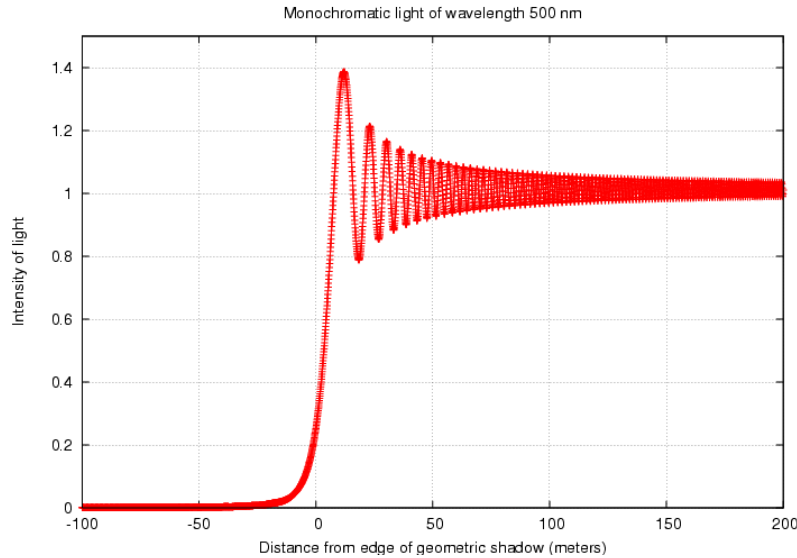


Figure 4.1: Simulation of model based on Eq. (4.1). Image credit goes to Michael Richmond. Note position of first fringe several meters *after* the edge.

the spacing between fringes  $b$  as

$$b = \sqrt{L\lambda} \quad (4.2)$$

where  $L$  and  $\lambda$  are still the screen-obstruction distance and the incident wavelength respectively. This condition is incompatible with the results for any line scans discussed in the previous chapter, so further analysis with this model was abandoned.

## 4.2 Beam Falling off Edge

Another model used to analyze the underlying nature of the “meta-peak” observed in  $I_{522}(x)$  is unrelated to Fresnel diffraction. The fundamental properties of this model are based on two basic statements:

- The Raman microprobe’s spot has finite width. The intensity of the probe is strongest at the center (point  $p$  in Fig. 1.6) of the spot and decreases radially. The profile of this beam is idealized to a circular Gaussian.<sup>4</sup>
- The intensity of the Raman signal backscattered from silicon is proportional to

---

<sup>4</sup>Siegman (1997)

the incident intensity of the exciting laser.<sup>5</sup>

For mathematical simplicity, the angular symmetry of the beam is used to reduce the problem to two-dimensions (as done in Fig. 1.6).

In the 2D case, the excitation laser's (ideal) spatial profile  $f(x)$  looks like a Gaussian centered at some point

$$f(x) = f_0 e^{-\frac{(x-p)^2}{2\omega^2}} \quad (4.3)$$

where  $f_0$  is the intensity at the center of the spot  $p$ .  $\omega$  is the Gaussian width parameter, related to the spot size by

$$d = \text{FWTM} = 2\omega\sqrt{2\ln(10)} \approx 4.3\omega . \quad (4.4)$$

As in the diffraction model, the  $I_{522}$  Raman band is proportional to the intensity of the excitation laser. If part of the beam is incident in the no-silicon region (i.e. after the edge,  $x > 0$ ) then no Raman scattering occurs – the no-silicon region contributes no  $I_{522}$ .

The Raman intensity of the  $522 \text{ cm}^{-1}$  mode at any given spot position  $I_{522}(p)$  then looks like

$$I_{522}(p) \propto I_0 \int_{-\infty}^0 e^{-\frac{(u-p)^2}{2\omega^2}} du + 0 \int_0^{+\infty} e^{-\frac{(u-p)^2}{2\omega^2}} du . \quad (4.5)$$

Here  $I_0$  is normalized to the intensity when the beam is far interior on the silicon ( $p \rightarrow -\infty$ ).<sup>6</sup>  $p$  still represents the spot's center, and  $\omega$  is the Gaussian width parameter from Eq. (4.4). The first term represents the  $I_{522}$  contribution for the region with silicon being excited and the second term is written to emphasize the *zero* contribution from the non-silicon region.

---

<sup>5</sup>Long (2002)

<sup>6</sup>This requires an additional normalization of the Gaussian integral so the integral equals 1 for the  $p \rightarrow -\infty$  condition. Eq. (4.5) is only expressing *proportionality*, so this normalization constant is omitted.

Calculating the area under the normal curve is not trivial. A function that serves as a shorthand for such an integral is the error function, defined as<sup>7</sup>

$$\text{erf}(x) \equiv \frac{2}{\sqrt{\pi}} \int_0^x e^{-u^2} du . \quad (4.6)$$

By clever substitution, the proportionality relation in Eq. (4.5) can then be written as

$$I_{522}(x) \propto \frac{A}{2} \left( \text{erf} \left( \frac{x-b}{\omega\sqrt{2}} \right) + 1 \right) \quad (4.7)$$

where  $A$  is a fitting parameter with intensity units (it absorbed  $I_0$ ),  $b$  offsets the line (so  $x = 0$  corresponds to the cleaved edge's position), and  $\omega$  is the same Gaussian width parameter from Eq. (4.4).

Eq. (4.7) is used to fit Edge 1 from the previous chapter and shown in Fig. 4.2. The best-fit parameters are given in Table 4.1.

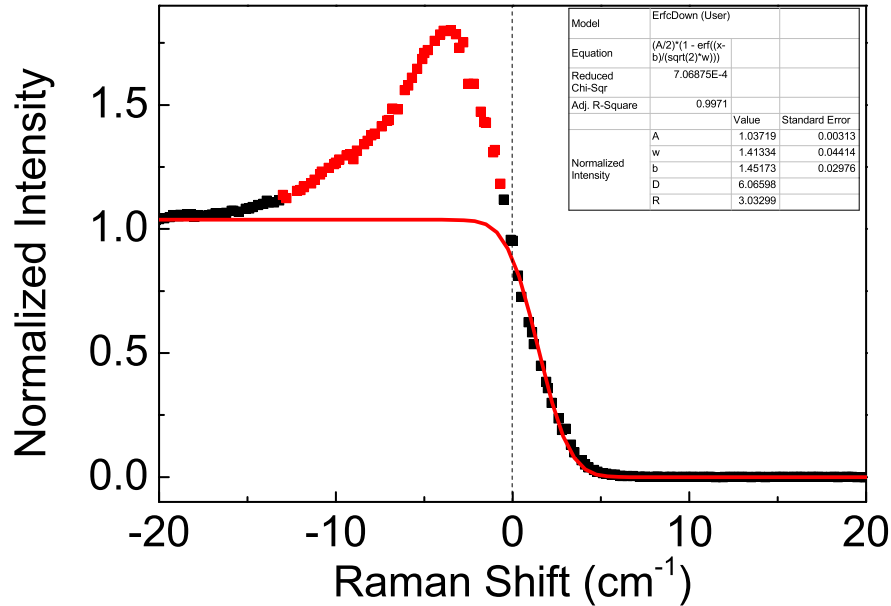


Figure 4.2: A numerical best-fit (red line) of Eq. (4.7) to the line scan from Edge 1. The red points indicate the region between points **A** and **C** from Table 3.1. During fitting, the red points were “masked” (essentially ignored). Best-fit parameters are given in Table 4.1.

---

<sup>7</sup>Weisstein (2015)

The most immediate shortcoming is the lack of a “meta-peak” produced by this model. This required fits to be done with a “mask” over the enhancement. By fitting Eq. (4.7) to several different edges, however, surprisingly reasonable estimations of spot size<sup>8</sup> were calculated from the best-fit’s value for  $\omega$ .

Parameter	Best-Fit Value	Std. Error
A	1.037	0.003
$\omega$	1.41	0.04
b	1.45	0.03

Table 4.1: Best-fit values of the parameters in Eq. (4.7) from the red line in Fig. 4.2.

This model uses an appealingly simple statement of proportionality to simulate  $I_{522}(x)$ . Unfortunately, its fitting parameters are difficult to assign physical meaning within the context of a line scan. Additionally, the model in no way accounts for the enhancement observed in most line scans. A simple modification made to Eq. (4.5) results in the starting point for the next, and more successful, model.

### 4.3 Edge Enhanced Simulation

As mentioned in the previous chapter, the surface density of silicon atoms varies with the cleavage plane of the edge. For each wafer orientation analyzed, the surface of the “slice plane” has the same surface density because they are cleaved along the [001] cleavage plane. The edges, however, are cleaved along different plane, thus they different surface densities.

When the beam traverses the cleaved edge, a small<sup>9</sup> portion of the edge’s “face” could be excited by the microprobe’s beam. If such a region is excited, its contribution to the Raman  $I_{522}$  measurement is not easy to determine. Rather, what if we simply say that the contribution near the edge could be *different* than the contribution from the interior?

As in the previous model, the probe’s spot is divided into many small area

---

<sup>8</sup>A similar model was constructed under the assumption the beam had a circular “top-hat” profile. Compared to that model’s horrendously poor estimations of spot size, the result here is reasonable.

<sup>9</sup>Exactly how much is difficult to determine. Small, here, simply means non-zero.

“chunks” ( $dAs$ ). Each of these “chunks” corresponds to a small region of silicon. Each “chunk” is also excited by the associated portion of the excitation laser’s beam profile. The excitation results in Raman scattering from the “chunk.” Again, the intensity of the excitation laser at that point is related to the intensity of the Raman signal contributed by that “chunk.” The measurement of  $I_{522}(x)$  is interpreted as the sum of the Raman signal from each of the area chunks.

Adding an additional term to Eq. (4.5) – one that accounts for a different Raman signal due to the edge face – and omitting the  $I_0$  constant, this new model can be expressed as

$$I_{522}(p) \propto \begin{cases} 1 * \int_{-\infty}^{-l} e^{\frac{-(u-p)^2}{2\omega^2}} du & \text{“Interior”} \\ +\lambda * \int_{-l}^0 e^{\frac{-(u-p)^2}{2\omega^2}} du & \text{“Edge”} \\ +0 * \int_0^{+\infty} e^{\frac{-(u-p)^2}{2\omega^2}} du & \text{“Off Edge.”} \end{cases} \quad (4.8)$$

The three terms are labeled with the region they represent and the “interior” & “off edge” terms are about the same as in Eq. (4.5), excepting the integration bounds. The second term introduces a new parameter  $\lambda$  (the *enhancement coefficient*) which allows the contribution in the region near the edge to be different than in the “interior” region. The  $l$  term used in the integration bounds determines the size of the “enhanced edge region.”

Unlike before, Eq. (4.8) is not straightforward to express with the error function. Multiple Python programs (the current version is featured in the Appendix) were constructed to numerically evaluate these integrals. The current version’s algorithm involves two additional parameters not yet discussed:  $N$  and  $t$ .

$N$  corresponds to the number of “steps”<sup>10</sup> ( $0.1 \mu\text{m}$ ) occupied by the enhanced region.

$t$  is a parameter used to generalize spot size, called a “threshold.” The full width at *tenth* maximum (FWTM) is usually the width connected with spot size –  $t = 0.1$  imposes this width connection in the algorithm. If the true spot width

---

<sup>10</sup>Referring to global step size. This is the  $\Delta x$  used to approximate the integral  $f(x) = \int g(x)dx \approx \sum_i g(x_i)\Delta x$ . In the program, the step size also determines the step between spot positions.

is in fact that full width at *hundredth* maximum, for example, the threshold can be adjusted to  $t = 0.01$ .

The behavior of this model can be analyzed by running many simulations and varying individual parameters. The results of these parameter variation tests are displayed in Fig. 4.3.

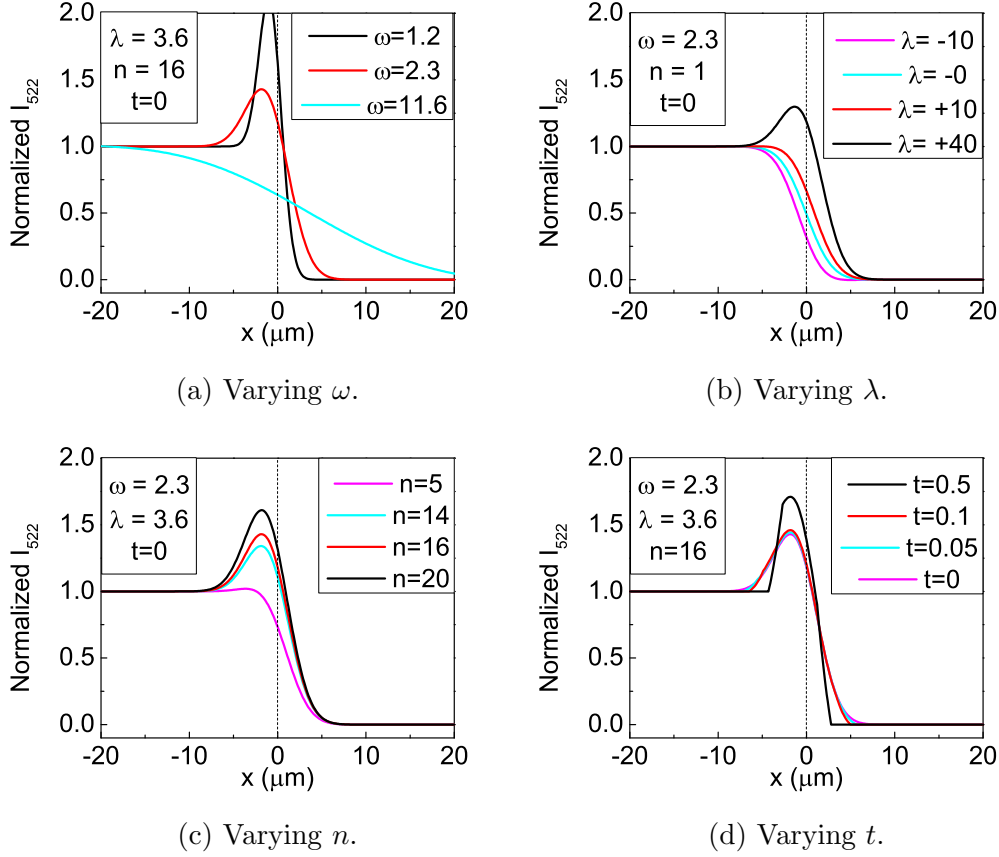


Figure 4.3: Simulations of the Edge Enhanced model using varied parameters. The chosen values for  $\omega$  correspond to the available objectives using Eq. (4.4) and Table 1.5. The other parameter ranges were chosen after fitted to data.

In Fig. 4.3a, the three values of  $\omega$  were chosen to reflect the three available objectives (100X, 50X, and 10X). Compared to line scans using these objectives (see Figs. 3.1 and 3.2), the result is roughly consistent with experimental data. The 10X scans ( $\omega = 11.6 \mu\text{m}$ ) appear to have no substantial enhancement of  $I_{522}(x)$ . The 100X ( $\omega = 1.2 \mu\text{m}$ ) and 50X ( $\omega = 2.3 \mu\text{m}$ ) scans, however have clear “meta-peaks.” Spot size clearly has a positive correlation with the simulated “meta-peaks.” This is

consistent with the second empirical relationship stated in the previous chapter.

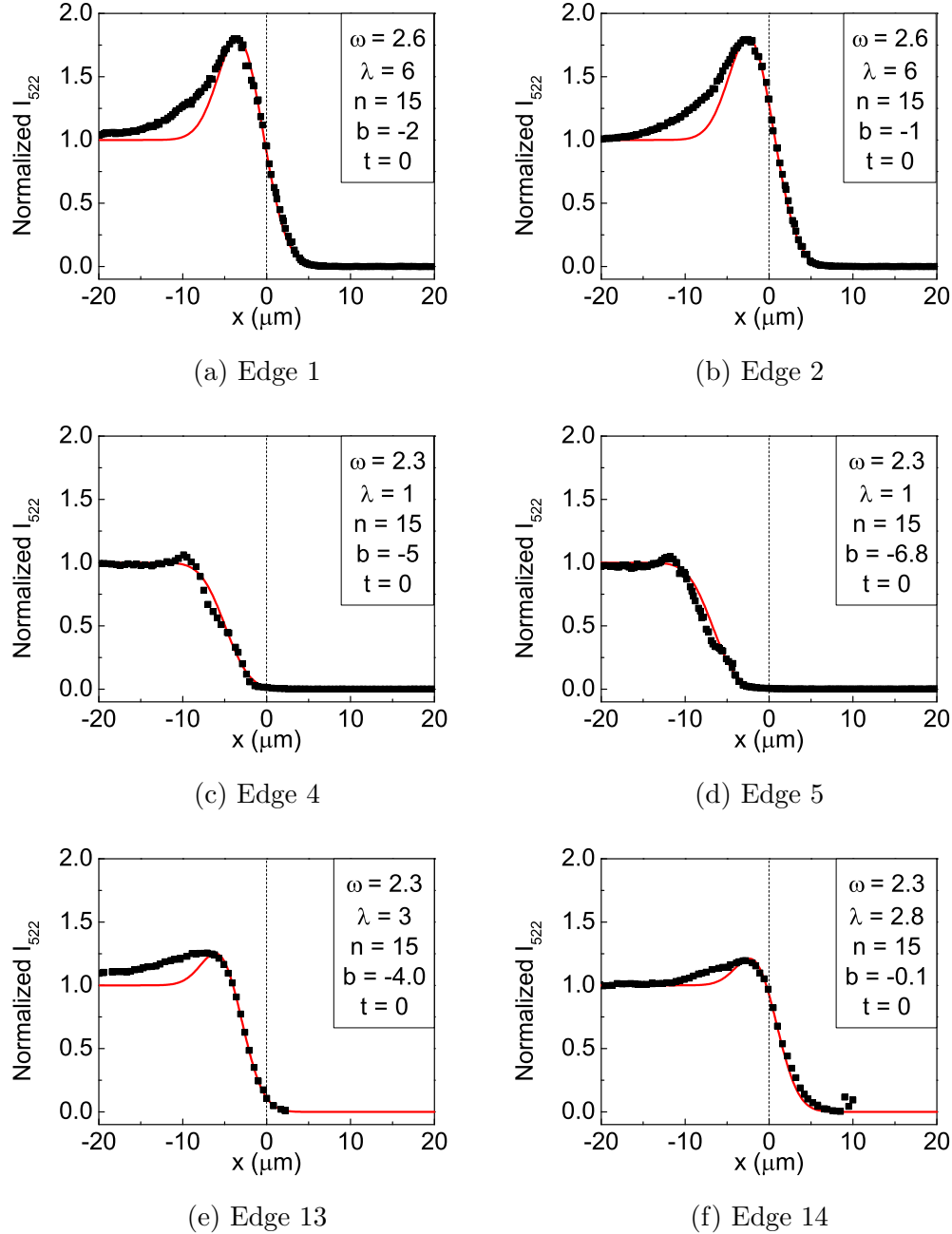


Figure 4.4: Multiple edge scans were visually fitted using the Edge Enhanced model. The inset boxes display the parameters for the model (red line). The best-fit values for  $\omega$  all roughly correspond to the 50X objective.

Edges 1, 2, 4, 5, 13, and 14 were “fitted” visually using the numerical simulation from this model. The “fitting” process amounted to running a simulation, visually

comparing the result to data, then running another simulation with a single parameter changed. The results of these “fits” are shown in Fig. 4.4.

In the fits shown in Fig. 4.4, the enhancement coefficient  $\lambda$  is the primary parameter adjusted to account for the different “meta-peaks.” The fits appear to account for the “drop” (the region after the “meta-peak”) much better than the error function alone.

In the scans with no “meta-peak,” Edges 4 & 5 (excitation wavelength of 532 nm), the fitted value of  $\lambda = 1$  yields essentially the same result as the error function model.  $\lambda = 1$  suggests that these edge scans show *no* edge enhancement.

The scans performed with an excitation wavelength of 785 nm (Edges 1, 2, 13, and 14) all exhibited some enhancement. Their respective fits show  $\lambda > 1$  to reflect this enhancement near the edge. The best-fit values of  $\lambda$  for Edges 1 & 2 are substantially larger than for Edges 13 & 14. This supports the suggestion that the cleavage plane of the edge plays a role in the enhancement of  $I_{522}(x)$ .

Similar fits have been performed using this model on all other scans reported here and many that were omitted with similar success seen above. The fitted values of  $\omega$  reflect the estimated spot sizes quite well, though statistics have not been collected.

The model appears to satisfy the empirical relationships established in the previous chapter. It should be applied cautiously, however, until the underlying natures of  $\lambda$  and  $n$  can be more explicitly characterized. For the purposes of estimating spot size and cleaved edge’s true position, this model has proven successful.

# Chapter 5

## Conclusion

In line scans across the cleaved edge of a silicon wafer, an enhancement is often observed in the intensity of the  $522\text{ cm}^{-1}$  Raman band. After extensive experimentation, three empirical relationships were established regarding this enhancement:

1. The enhancement is more intense with a longer excitation wavelength. Scans performed with a 532 nm beam showed no substantial “meta-peak.” By contrast, scans with the 785 nm beam had “meta-peaks” maxing out at 80% above the normalized interior intensity.
2. The enhancement is less intense with a larger spot size. Scans using the 10X objective showed virtually no enhancement. 50X and 100X scans, however, show very clear “meta-peaks.”
3. Smaller spot size results in  $I_{522}(x)$  dropping to zero more quickly. In 100X scans,  $I_{522}(x)$  decreased from maximum to 50% in less than  $2\text{ }\mu\text{m}$ . For 10X scans, this decrease occurred over greater than  $10\text{ }\mu\text{m}$ .

Additionally, scans performed on edges cleaved along the (110) plane had less intense “meta-peaks” than their (001) counterparts.

The most successful attempt at modeling the enhancement of  $I_{522}(x)$  did so without consideration of diffraction or grain size. Numerical simulations with carefully chosen parameters yield plots of  $I_{522}(x)$  that share many features with experimental results. The parameters determined by these “visual fits” have values which seem to correspond with the experimental conditions. Notably, the spot size of the 50X objective is fitted closely to its reported value of about  $10\text{ }\mu\text{m}$ .

With further refinement and analysis of the Edge Enhanced model, it seems possible to detect the true edge with high accuracy. Given the objective, excitation wavelength, and orientation of the wafer, a simulation could calculate  $I_{522}(x = 0)$ . This value could then be used to identify the position of the cleaved edge.

# Fityk Script Generator

```
"""
Name: fitykScriptGenerator_v3
Authors: Andrew Fiorillo & Dr. Brian Hosterman

Purpose: Searches for all folders beginning with a '=' symbol
in the CWD and iterates through each matched folder. Each
matching folder containing .PRN files (Raman spectra) will have
a script generated to process all files in the folder. Processing
includes subtracting the background signal, inserting a Voigt peak
near 522 cm^(-1), and using a fitting algorithm to refine the peak.
Parameters are outputted to an output text file.

"""

import os, os.path

def main():
    """ Checks the directory for subdirectories and .prn files"""
    listMain = os.listdir(os.getcwd())
    dirsMain = []
    for item in listMain:
        if '=' in item: dirsMain.append(item) #List only directories with =

    for dr in dirsMain:
        os.chdir(os.getcwd()+'\\'+dr)
        genFile()
        os.chdir('..')

def genFile():
    """ Generates Fityk script to process all PRNs in CWD."""
    # SET ACTIVE RANGE AND ZOOM
    active_range = 'A = (x > 100 and x < 1000)'
    zoom = 'plot [50:1050] []'

    # SET BACKGROUND
    background = '%bg0 = Spline(\n'
    argmin(y if x > 200 and x < 250),min(y if x > 200 and x < 250) \
    , argmin(y if x > 400 and x < 450),min(y if x > 400 and x < 450) \
```

```

    , argmin(y if x > 650 and x < 700),min(y if x > 650 and x < 700))\
    , argmin(y if x > 800 and x < 900),min(y if x > 800 and x < 900))'

listFiles = os.listdir(os.getcwd())
prns = []
for item in listFiles:
    if '.prn' in item.lower():
        #print item
        prns.append(item)
if prns == []:
    print 'Oh No!'
    print os.getcwd()
filename_prefix = (prns[0])[0:-11]

info_filename = filename_prefix+'.txt'

# GENERATE!

_script_name = '_script_' + filename_prefix.lower() + '.fit'
fout = open(_script_name, 'w')

for spectra in prns:
    # Load new file
    load_string_prefix = "@0 < '_EXECUTED_SCRIPT_DIR_/'"
    load_string = load_string_prefix + spectra + ""

    fout.write(load_string + '\n')
    # Set active range
    fout.write(active_range + '\n')
    # Set background
    fout.write(background + '\n')
    # Subtract background
    fout.write('Y = y - %bg0(x)\n')
    # Subtract Negative Values
    fout.write('Y = max2(y, 0)' + '\n')
    # Zoom in on active range
    fout.write(zoom + '\n')
    # If first spectrum, guess Voigt around 522cm^-1
    if spectra == prns[0]:
        fout.write('guess Voigt[500:550]+'\n')
    # Run fitting algorithm 20 times
    fout.write('fit\n' * 10)
    # save info to info_filename
    save_location = "'_EXECUTED_SCRIPT_DIR_/" + info_filename + "'"
    # if this is the first spectra, create a new file

```

```
# overwriting if old exists
if spectra == prns[0]:
    fout.write('info filename > ' + save_location + '\n')
else:
    fout.write('info filename >> ' + save_location + '\n')
fout.write('info peaks_err >> ' + save_location + '\n')
fout.write("print 'Processed Spec " + str(spectra) + "'\n")
fout.write('\n')
#print 'Spectra', spectra, 'fitting script generated.'

fout.close()
print _script_name, 'generated in', os.getcwd()

main()
```

# “Peaks”

```
# -*- coding: cp1252 -*-
# Author: Brian D. Hosterman
# Graphing capabilities added by Nick Abboud
# Converted output to CSV format and implemented
# support for to import coordinates from scandata.txt - AF
# last edited on 22 September 2014
#
# This python script will reformat a Fityk data file containing
# the output of ==> info peaks_err >> filename.txt
#   "_script.fit" is the fityk script used
# Calculates peak areas and uncertainties
#
# This script should deal with Lorentzian, Gaussian, Voigt, and
# SplitVoigt functions properly
#
#
# It also rounds off all numbers to 4 digits
# I don't think this should be a problem for any parameters.

import math
import sys # add command line options
import os
import numpy as np
import matplotlib.pyplot as plt # these are for plotting

# ...

def cal_u_fwhm_voigt(gwidth, u_gwidth, shape, u_shape):
    # if voigt, need to do error propagation to calculate u_fwhm
    # However, if shape is really small, the relative uncertainty is
    # ridiculously big, and since a small shape means the parameter is
    # 0, we will zero out u_shape for really small shapes
    if shape < 0.01:
        u_shape = 0.0
    # hwhm_voigt = 0.5346 w_l + sqrt(0.2169 w_l^2 + w_g^2)
    # where w_l and w_g are hwhm, NOT fwhm
    # gaussian width, w_g = sqrt(ln(2)) * gwidth
```

```

#    lorentzian width, w_l = shape * gwidth
b = math.sqrt(math.log(2))
# fwhm is a function of gwidth and shape, so...
#    pfpg / pfps : partial fwhm, partial gwidth / partial shape
#    root : sqrt(0.2169 shape^2 + b^2) term that shows up
root = math.sqrt(0.2169 * shape**2 + b**2)
pfpg = 0.5346 * shape + root
pfps = 0.5346 * gwidth + 0.2169 * gwidth * shape / root
u_fwhm = 2 * math.sqrt( pfpg**2 * u_gwidth**2 + pfps**2 * u_shape**2 )
return u_fwhm

# ...

def cal_fwhm_voigt(gwidth, shape):
    # hwhm_voigt = 0.5346 w_l + sqrt(0.2169 w_l^2 + w_g^2)
    # where w_l and w_g are hwhm, NOT fwhm
    w_g = math.sqrt(math.log(2)) * gwidth
    w_l = shape * gwidth
    hwhm_voigt = 0.5346 * w_l + math.sqrt(0.2169 * w_l**2 + w_g**2)
    return 2 * hwhm_voigt

# ...

# k_g: w_g / (w_g + w_l) = 1 / (1 + 1.20087 shape)
# This is similar to shape, but used in the area_voigt calculation
def cal_k(shape):
    b = math.sqrt(math.log(2))
    return b / (b + shape)

# u_k_g
def cal_u_k(shape, u_shape):
    b = math.sqrt(math.log(2))
    return b * u_shape / (b + shape)**2

# area_voigt
def cal_area_voigt(height, gwidth, shape):
    # I found a paper describing how to approximate voigt area as
    # A = c * height * fwhm
    # where c = 1.572 + 0.05288 k - 1.323 k^2 + 0.7658 k^3
    # and k = w_g / (w_g + w_l)
    k = cal_k(shape)
    c = 1.572 + 0.05288 * k - 1.323 * k**2 + 0.7658 * k**3
    area_voigt = c * height * cal_fwhm_voigt(gwidth, shape)
    return area_voigt

```

```
# u_area_voigt
def cal_u_area_voigt(height, u_height, gwidth, u_gwidth, shape, u_shape):
    k = cal_k(shape)
    u_k = cal_u_k(shape, u_shape)
    c = 1.572 + 0.05288 * k - 1.323 * k**2 + 0.7658 * k**3
    u_c = (0.05288 - 2 * 1.323 * k + 3 * 0.7658 * k**2) * u_k
    area_voigt = cal_area_voigt(height, gwidth, shape)
    u_h_rel = u_height / height
    u_k_rel = u_k / k
    u_c_rel = u_c / c
    return area_voigt * math.sqrt(u_h_rel**2 + u_k_rel**2 + u_c_rel**2)

# ...
```

# Edge Enhanced Model

```
# -*- coding: utf-8 -*-
import numpy as np
import matplotlib.pyplot as plt
global bound,step
bound=25
step=0.1
plt.ion()

w=2.3
b=0
coeff=50
n=1
gap=5

x = np.arange((-1*bound),bound,step)

def partInt(x,pos,w,profile='Gauss'):
    """ Returns a 2D array of dA chunks. The sum of dAs is the integral.
    Parameters:
        x: (np.array), shape (1,2*bound)
            Global x-coordinates
        pos: (float)
            Position of center of beam in microns
        w: (float)
            Gaussian width parameter (FWTM=4.3*w)
    Returns:
        areas: (np.array), shape (2,2*bound)
            areas[0] returns the x-coordinates again
            areas[1] returns the dA chunk at the position
    """
    if profile.lower()=='gauss':
        y = (np.exp(-((x-pos)**2)/(2*w**2)))
    else: #For other beam profiles, maybe a Bessel?
        pass
    dAs = y*step
    return np.vstack((x,dAs))
```

```

def imposeSpot(x,areas,threshold,info=False):
    """ Sets each dA value < (dA_max*threshold) to zero.

    Parameters:
        x: (np.array), shape (1,2*bound)
            Global x-coordinates
        areas: (np.array), shape (2,2*bound)
            Array generated by partInt() containing dA chunks
            areas[1] contains the dA chunks
        threshold: (float)
            Minimum percentage of maximum to allow in integral
            threshold=0.1 yields an array of dAs only over FWTM region
        info: (boolean, optional)
            If True, changes returned values to include a tuple with spot size

    Returns:
        (spotAreas,spotSize): (tuple)
            spotAreas: (np.array), shape (2,2*bound)
                spotAreas[0] returns the x-coordinates again
                spotAreas[1] returns the dA chunks greater than dA_min
            spotSize is the width of the allows dA chunks in microns
    """
    dAs = areas[1]
    dA_max = np.max(dAs)
    dA_min = dA_max*threshold
    mask = (dAs >= dA_min) # Array of Trues only where dA>dA_min, else False
    if info==True:
        spotSize = np.count_nonzero(dAs*mask)*step
        return (np.vstack((x,dAs*mask)),spotSize)
    return np.vstack((x,dAs*mask))

def genStage(x,coeff,n,gap=False):
    """ Returns a 2D array of enhancement coefficients.

    Parameters:
        x: (np.array), shape (1,2*bound)
            Global x-coordinates
        coeff: (float)
            Enhancement coefficient (to be multiplied by respective dA chunk)
        n: (int), must be n>=1
            Number of chunks to possess enhancement coefficient
        gap: (float, optional)
            Width of gap in microns
            Implies a slit configuration

    Returns:

```

```

stage: (np.array), shape (2,2*bound)
    stage[0] returns the x-coordinates again
    stage[1] returns the respective enhancement coefficient
"""
stage = np.ones(len(x)) # Starts with a stage with no physical edge

for i in xrange(len(x)):
    if x[i]>(-(n-1)*step) and x[i]<step: # enhancement before and at edge
        stage[i] = coeff
    elif x[i]>0 and gap==False: # From edge to end of coords (simple edge)
        stage[i] = 0
    elif x[i]>0 and x[i]<gap: # From physical edge to end of gap
        stage[i] = 0
    elif x[i]>gap and x[i]<=(gap+n*step): # n*step wide chunk on 2nd edge
        stage[i] = coeff
return np.vstack((x,stage))

def scan(x,w,coeff,n,threshold,gap=False, debug=False):
    """ Returns a 2D array of a simulated I_525(x)

Parameters:
    x: (np.array), shape (1,2*bound)
        Global x-coordinates
    w: (float)
        Gaussian width parameter (FWTM=4.3*w)
    coeff: (float)
        Enhancement coefficient (to be multiplied by respective dA chunk)
    n: (int), must be n>=1
        Number of chunks to possess enhancement coefficient
    threshold: (float)
        The percentage of beam intensity that's
    gap: (float, optional)
        Width of gap in microns
        Implies a slit configuration, if False then a simple edge

Returns:
    scan: (np.array), shape (2,2*bound)
        scan[0] returns the x-coordinates again
        scan[1] returns I_525(x)
"""
bigX = np.arange((-2*bound),2*bound,step) #Extends x-range to trim later
stage = genStage(bigX,coeff,n,gap)
if debug==True: print stage.T

```

```
intensities = np.zeros(len(bigX))
for i in xrange(len(bigX)):
    pos = bigX[i]
    areas = partInt(bigX,pos,w)
    spot = imposeSpot(bigX,areas,threshold)
    intensities[i]=np.sum(spot*stage)

#Trim off excess and normalize
trim = bound/step
outX = bigX[trim:(-trim)]
outI = intensities[trim:(-trim)]
if gap==False:
    outI = outI - outI[-1] #Off the wafer ought be zero
else:
    outI = (outI - outI[0] + 1) #Subtract constant added to all points
    outI = (outI>0)*outI #Make any negative values 0
outI = outI / outI[0] #Normalize

if debug==True: print 'outI:\n',outI

if gap!=False:
    scan = np.vstack((outX,outI))
    return centerSlitScan(scan,gap)

return np.vstack((outX,outI))
```

# Bibliography

- Fujitsu (2008). Fujitsu Laboratories Develops Power-Saving CMOS Technology for 32nm-Generation and Beyond. Technical report, Fujitsu, Kawasaki. <http://www.fujitsu.com/global/about/resources/news/press-releases/2008/1216-01.html>.
- Griffiths, D. (2005). *Introduction to Quantum Mechanics* (2nd ed.). Pearson Prentice Hall.
- Hecht, E. (2002). *Optics* (4th ed.). Addison-Wesley.
- Kaiser Optical Systems, I. Introduction to Raman Spectroscopy. [http://www.kosi.com/na\\_en/products/raman-spectroscopy/raman-technical-resources/raman-tutorial.php](http://www.kosi.com/na_en/products/raman-spectroscopy/raman-technical-resources/raman-tutorial.php).
- Kittel, C. (2004). *Introduction to Solid State Physics* (8th ed.). Wiley.
- Long, D. A. (2002). *The Raman Effect: A Unified Treatment of the Theory of Raman Scattering by Molecules*. Wiley.
- Mathew, A. (2006). Lattice Vibrations – Phonons in Solid State. *Workshop on Advanced Topics in Semiconductor Devices2*, 1–3.
- Misra, P. (2011). *Physics of Condensed Matter* (1st ed.). Academic Press.
- NIST (2010). Lattice Parameters of Silicon. <http://physics.nist.gov/cgi-bin/cuu/Value?asil>.
- Nova Electronic Materials, I. (2014). About Silicon. <http://www.novawafers.com/resources-about-silicon.html>.
- Prime Wafers, I. (2015). How to Cleave a Wafer with a Diamond Scribe. [http://primewafers.com/Cleave\\_with\\_a\\_diamond\\_scribe.html](http://primewafers.com/Cleave_with_a_diamond_scribe.html).
- Raman, C. (1930). The molecular scattering of light. In *Nobel Lectures, Physics 1922-1941*, Amsterdam, pp. 15. Elsevier Publishing Company.
- Reusch, W. (2013). Infrared Spectroscopy.
- Richmond, M. (2005). Diffraction effects during a lunar occultation. <http://spiff.rit.edu/richmond/occult/bessel/bessel.html>.

- Rottenfusser, R., E. Wilson, and M. Davidson. Education in Microscopy and Digital Imaging. <http://zeiss-campus.magnet.fsu.edu/articles/basics/>.
- Siegman, A. E. S. U. (1997). How to ( Maybe ) Measure Laser Beam Quality. In *Optical Society of America Annual Meeting*, Long Beach, pp. 1–18.
- Sikora, L. (2011). Properties of silicon and silicon wafers. <http://www.el-cat.com/silicon-properties.htm>.
- Weisstein, E. W. (2015). Erf.
- Wojdyr, M. (2010). Fityk: A general-purpose peak fitting program. *Journal of Applied Crystallography* 43, 1126–1128.
- Wojdyr, M. (2014). *Fityk User's Manual*. <http://fityk.nieto.pl/fityk-manual.html>.
- Wright, D., P. Greve, J. Fleischer, and L. Austin (1992). Laser beam width, divergence and beam propagation factor—an international standardization approach. *Optical and Quantum Electronics* 24, 993–1000.
- Xu, S., X. Tang, Y. Yue, and X. Wang (2013, November). Sub-micron imaging of sub-surface nanocrystalline structure in silicon. *Journal of Raman Spectroscopy* 44(11), 1523–1528.